People's Democratic Republic of Algeria
Ministry of Higher Education and Scientific Research

University M'Hamed BOUGARA – Boumerdès

Institute of Electrical and Electronic Engineering
Department of Electronics

Project Report Presented in Partial Fulfilment of

the Requirements of the Degree of

'MASTER'

In Power Engineering

Title:

Droop-controlled single phase AC Microgrid using SOGI-PLL

Presented By:

- **DIAF Hadil**

Supervisor:

Pr. KHELDOUN Aissa

Registration Number:...../2022

Abstract

A microgrid (MG) is defined as a low or medium voltage distribution network that is also connected to a number of distributed generation sources, energy storage elements, and controllable loads.
A MG can operate both in grid-tied mode, when its bus is connected to the main grid, or in islanded more, when it's disconnected.
MG control strategy is considerably different than that of the traditional grid. A hierarchical control architecture consisting of primary, secondary, and tertiary control is adopted to regulate voltage and frequency and ensure a stable and reliable network.
In order to offer a good power quality for end users in islanded microgrids, the power sharing between distributed generators (DGs) is the first challenge that must be dealt with. In this report, a droop control method based primary control for two parallel single-phase VSIs forming an islanded microgrid is presented.

The controller aims to ensure optimal power sharing between different DGs using modified droop-control technique and introducing SOGI-PLL for parameter estimation and DC-offset rejection, during islanded operation.

Key words : Microgrid, hierarchical control, droop-control, SOGI-PLL, power sharing

Dedication

First and foremost, I would like to dedicate this work to myself, above all, for being strong and dedicated and not giving up in the hardest times.

To my beloved mother, who has always been my anchor and ray of hope, and never doubted me or my potential, and without whom I wouldn't be who I am today. I hope you will be able to witness all of my successes, for they will all be dedicated to you, always.

To my beloved father, who has always been a great listener and supporter. I wouldn't have gone through half the challenges if it weren't for his guidance and love. May you always be my side at the most critical points in my life, for I only have the courage to make big decisions when you are with me.

To my silbings whom I love so much, my brother Sari and my sister Dacine, with whom I shared my most memorable moments.

To my friends who listened to me talk nonstop about my thesis and never complained of my obsession nor my complaints whenever a simulation fails.

To my partner in everything, my best friend and the person I cherish the most, Mohamed Mohammedi. The one person who never hesitated to stop everything and come to my help, even when I don't ask for it. The one who put up with me, even during the days I couldn't put up with myself. To you, may you always be my guiding light when all goes dark.

Acknowledgement

My sincerest gratitude goes to my family, who has always stood by me and believed in my potential, even when I didn't. They are the reason I am here today, despite the rough months I have gone through due to my severe health issues.

I would like to extend my warmest thanks to my friends, Anfel Badaoui, Inas Koufi and Lina Kebaili for their constant support during these times of need and insecurity. Your understanding and committment is what kept me safe and sound even when I reached the verge of sanity. Thank you for listening, guiding, and loving me, even in my worst. Thank you for believing me and in my work, for always being there, regardless of everything.

And last but not least, I would like to thank my supervisor, Pr. Aissa Kheldoun, for his constant support and understanding, I am fortunate to have you as a supervisor and mentor, and I hope I will have the chance to work on further research with you.

Contents

List of Tables

List of Figures

List of Symbols and Abbreviations

Ω	Ohm - resistance unit
A	Amperes - Current unit
AC	Alternative Current
C	Capacitance
DC	Direct Current
DG	Distributed Generation
EPS	Electrical Power System
ESS	Energy Storage System
F	Farad - Capacitance unit
f	Frequency
H	Henry - Inductance unit
I	Current
L	Inductance
MG	Micro-Grid
PI	Proportional Integral
PLL	Phase Locked Loop
PR	Proportional Resonant
PV	Photo-voltaic
R	Resistance
RES	Renewable Energy Source
$SOGI$	Scond Order Generalized Integrator

TDA Traditional Droop Approach

THD Total Harmonic Distortion

V Voltage

VSI Voltage Source Inverter

W Watt

General introduction

The trends towards renewable energy sources (RES), has increased considerably, due to the global incessant rise in power demand. Among all RES, photovoltaics (PV) and wind turbines; in particular, have received the most attention. The main reason for this unexpected growth in the use of RES, beside answering the high demand for electricity, is the attempt to alleviate the emissions of CO_2 from burning fossil fuel-based electricity production; and achieve a sustainable supply of energy, especially after the Paris agreement that took place in 2015.
The European Union's (EU) energy policy has made it one of the world leaders in the promotion of renewable energy [1]. Besides the EU, Canada has shown some admirable commitment to RES integration, as the power generation from RES was extended to 30% [2].

However, one major issue RES suffer from is the intermittent nature of generation, in addition to the need for power electronics converters before their electricity can be injected to the network.

To answer the aforementioned problematic, the concept of microgrids (MG) was introduced to facilitate the integration of distributed generation without the need to install new transmission lines.

However, since MGs are comprised of RES, they suffer from unreliability as they rely on non-dispatchable sources that are subject to changes depending on the environment conditions. To this end, a hierarchical control strategy is used to ensure stable and reliable power in MGs, both in their islanded and grid-connected modes.

In the islanding mode of operation of MGs, the demand power should be shared among the different DGs considering their capacity to ensure balance and longer life-time of the DGs in use.

The purpose of this work is the design of a robust efficient primary controller for an islanded AC MG that ensures a good power quality and power balance between the DGs.

This report details the design of the said controller along with the simulation results

under different scenarios to test its efficiency in three chapters.
First, a theoritical background about MGs, their different topologies and a comprehensive overview of the different control strategies used at each level is covered. In the following chapter, Chapter II, the proposed model of the MG in addition to the different stages of the controller design are presented in details. The simulink model of the system is provided in Chapter III, followed by the simulation results describing the behavior of the MG under different load conditions. Finally, future works and further developments are discussed for the sake of guiding students who wish to continue the work on MG control.

Chapter 1

Microgrids: classification and control strategies

1.1 Introduction to Microgrids

Distributed generation (DG) has been receiving significant attention lately. This comes as no surprise for DG was found to be an effective solution for the worldwide problematic of increasing load demand. DG aims to reduce the stress on the existing and extensive transmission and generation system. While the interest in DGs has only spiked in the recent years, the concept of DG actually dates back to the early 1990's. It mainly depends on the installation and operation of a portfolio of small size and clean electric power generating units interconnected at nearly any point in the power system [3].

A DG can be comprised of any emerging micro-generating technology, from fuel-cells to PV and wind turbines. One of their most praised advantages is that the power can directly flow from the source to the customer without requiring to go through the transmission network. In addition to that, DGs also ensure that the loads are served even if the transmission network is down in the case of faults. However,many issues should be dealt with. The need for electronic power converters is an issue, which needs to be addressed for the integration of renewable energy resources into the electric grid and play a significant role with the key control objectives [4].

Furthermore, the lack of low inertia of DG units is also considered one of the most important challenges facing these systems. It can lead to some serious power unbalances between the generation and load. In addition to that, the output of renewable energy resources fluctuates with the weather conditions, which can be an important issue when DG units are connected to the utility grid.

To cope with the above-mentioned issues and exploit distributed RESs more efficiently, the concept of microgrids was introduced as a new paradigm for the future power distributed generation systems, and the future of the power system as a whole.

According to the U.S. Department of Energy (DOE), a microgrid is defined as, "A group of interconnected loads and distributed energy resources within clearly defined electrical boundaries that acts as a single controllable entity with respect to the grid. A microgrid can connect and disconnect from the grid to enable it to operate in both grid-tied and islanded mode" [5].

1.2 Advantages of microgrids

MGs have been adopted as a way to utilize DG more efficienty for their numerous advantages, from which we cite the following:

- Facilitating distributed generation (DG) and allowing the use of renewable energy sources at their original location [6]

- Reducing transmission line losses by making the generation source close to the customer, thus relieving the customer from additional transmission system
- Increasing the power quality and improving the overall reliability of the electric supply by providing the ability to disconnect during faults in the MG or the utility grid
- Easing the use of flexible loads, and ensuring more precise matching between the generation and the power demand. This improves the power system efficiency and defers the need for grid reinforcements
- Presenting a cost-effective way to facilitate rural electrification, as no main power system extension is needed to operate the MG

1.3 Microgrids operation modes

Generally, the MG network can operate in two distinct modes: either in a grid-tied mode or a stand-alone mode feeding critical loads or rural customers who are not connected to the main grid[7].

1.3.1 Grid-connected operation

In this mode of operation, the MG is coupled to the utility grid through a static transfer switch.
The connection point is called point of common coupling (PCC). The MG controller continuously monitors the generation and demand in the MG. In case of power excess, it is exported to the grid. When on there is a power deficiency, electrical power is imported to the MG through the inverter, depending on the load and source conditions [8].

1.3.2 Islanded operation

As the name suggests, in this mode, the MG is completely disconnected from the utility grid.
The control of MG becomes much more complex, as the system becomes extremely sensitive to fluctuation both in generation and load variation, due to the low inertia of the system [9]. The VSIs control autonomously the local voltage and frequency of the MG. They must ensure the active and reactive power balance in addition to generation and demand balance.
This is met using different control strategies such as master-slave control method, control area network communication, or voltage and frequency droop strategy based on local measurements [10].

1.4 Microgrids architecture

As discussed in the previous sections, the MG network can either operate in grid-tied or stand-alone mode.

According to the MG functionalities and type of interconnecting at the common bus, MG can be classified as AC MGs, DC MGs, and hybrid MGs [11]. The different architectures are further elaborated in the sections below.

1.4.1 DC Microgrids

The concept of DC MG has been receiving significant interest in smart-grid research thanks to its efficiency, reliability, and simplicity [12].
In a DC MG, the different distributed generators are connected to the DC bus only through a single-stage voltage transformation device. This structure is more economical in cases where there are many DC power sources and loads, in the case of having PV systems and fuel cells. Since a large number of RESs with DC characteristics in nature, such as solar PV panels and electric vehicles (EVs), have been increased steadily in smart cities, the DC MG has become more attractive and gained much attention in recent years [13].
The DC MG can be either connected to the traditional AC distribution network through DC to AC conversion or to the high-voltage DC distribution network.

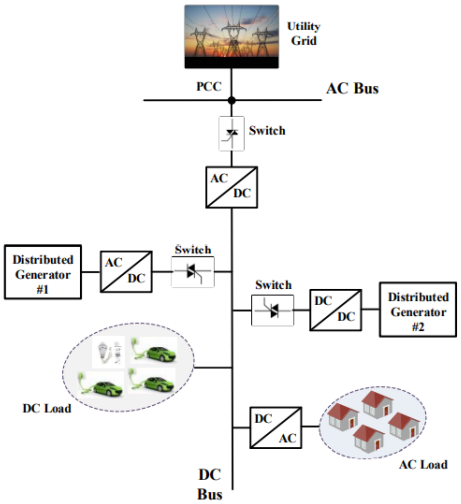

Figure 1.1: Topology of a DC Microgrid

1.4.2 AC Microgrids

In an AC microgrid architecture, the distributed generators are connected to an AC common bus through power electronic converters.
AC MGs are more taken into account in research as they present several challenges in voltage

amplitude and frequency controls, both active and reactive power flows, in addition to the connection to the utility grid [14].

This architecture is mostly adopted when the majority of the power sources in the MG generate AC voltages that can match the grid level through interfacing power converters. In such an AC-coupled local power system, the main power management requirement is to ensure that the power generated meets the load requirement. This issue becomes more important in the islanded operation mode, as the main control objective becomes the stabilization of AC bus voltage in terms of both frequency and amplitude.

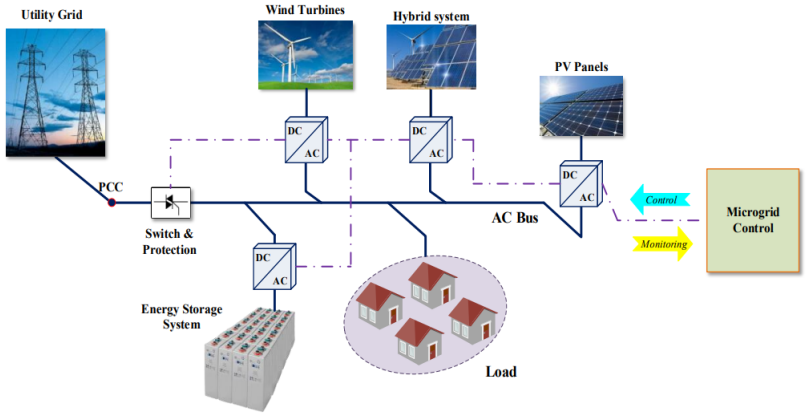

Figure 1.2: Topology of an AC Microgrid

1.4.3 Hybrid Microgrids

Hybrid MG systems are designed to acquire advantages from both the AC and DC MG. They are composed of two separate AC and DC sub-grids[15]. Both DC and AC buses can be attached with DERs and ESSs, and these buses are interconnected by interlinking converters.

Unlike the DC MG, the AC–DC hybrid MG DERs and ESSs are connected to an AC bus, which requires even more complex coordination for the voltage and power control between the DC and AC sub-grids.

However, they do have one similarity to the DC-coupled MG. Parallel interlinking converters are needed to interconnect the AC and DC buses in order to increase capacity and reliability.
Generally, this configuration is considered in the case where most of the power sources include a combination of both DC and AC power sources. This way, the overall efficiency is improved and the system costs are also reduced significantly. By connecting sources and

loads to the AC and DC buses, the number of power converters is reduced, and hence, the power conversion requirements, can also be minimized.

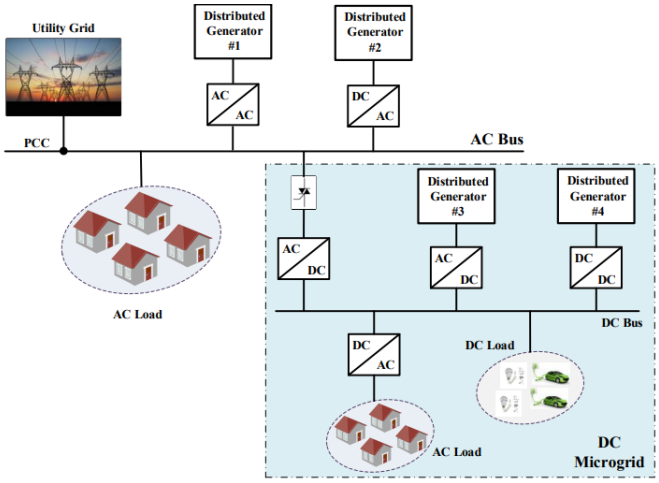

Figure 1.3: Topology of a hybrid Microgrid

1.5 Microgrids Application

1.5.1 Space microgrids

Satellites require an intricate design and are often burdened with a lot of tradeoffs. Among those are the spacecraft development time and cost, in addition to launch.
In order to overcome the aforementioned issues, small satellites such as nanosatellites and picosatellites, known as CubeSats,have been proposed and developed, and have been receiving quite the interest lately.

This specefic class of satellite only orbits in the low-Earth orbit (LEO) and have proven to be perfectly able to perform most of the tasks associated with larger satellites.
Furthermore, they have even been used in exoplanets as well, as they orbit in the low orbits of other planets like Mars [16].

The main components of satellites is the Electrical Power System (EPS). It is responsible for the power generation, storage, delivery, and conditioning.
If any of these is deficient, satellites would be out of service and could even cause the failure of the whole space mission.

The strict requirements of the satellites' EPS, from its limited weight and space, impossibility of repair, wide range of temperatures, to the severe radiation environment it will subject to, has given it great attention from researchers. Th

These requirements can be fulfilled by a number of control methods to create a robust, resilient design of the EPS [17].

For energy generation, CubeSats are, in most cases, equipped with PV solar cells. However, there have been other developments, such as radioisotope technology in interplanetary missions [18].

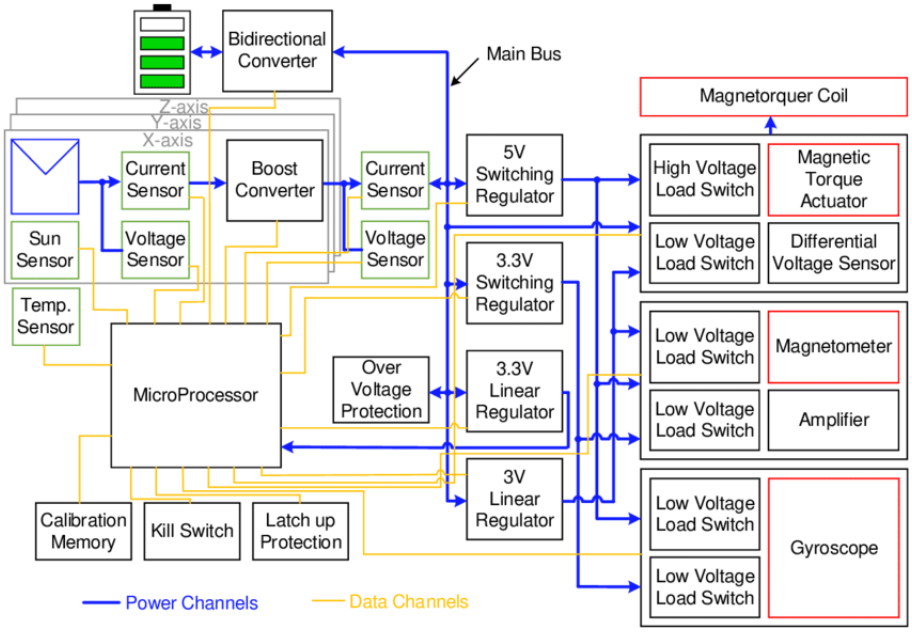

Figure 1.4: The overall structure of the CubeSat [17]

Even though solar PVs are the most employed for energy generation in CubeSat, they have numerous drawbacks, the most important one being their dependency on solar irradiance. For instance, the generated power is null during the eclipse, while it is variable in the presence of sunlight. To ensure the continuous operation of the CubeSat, batteries are employed as a backup and charged during high solar irradiance levels, when the power generated by the solar arrays is higher than the load's power. The batteries are used to generate energy during the the eclipse, as they can also be used even during high solar irradiance in the case of peak loads.

1.5.2 Shipboard microgrids

Shipboard MGs are one of the most recent applications of DGs. While Shipboard MGs are recent, the electrification of ships can be dated back to the early 20th century.

In the following century, the shipboard power systems (SPSs) have seen a great evolu-

tion in both size and power level.

The concept of all-electric ships that rely strictly on electric propulsion systems and integrated power systems (IPSs) has drawn great attention shipbuilding industry globally, due to the flaming prices of fossil fuels and the regulation of emission from the government and international organizations (i.e. IMO) that are only becoming stricter.

With the integration of energy storage systems (ESSs) and RES into SPSs in an effort to reduce sailing cost, the shipbaord electrical system becomes even more consist with MGs. In this context, the IPSs can indeed be defined as shipboard microgrids (SMGs) [19].

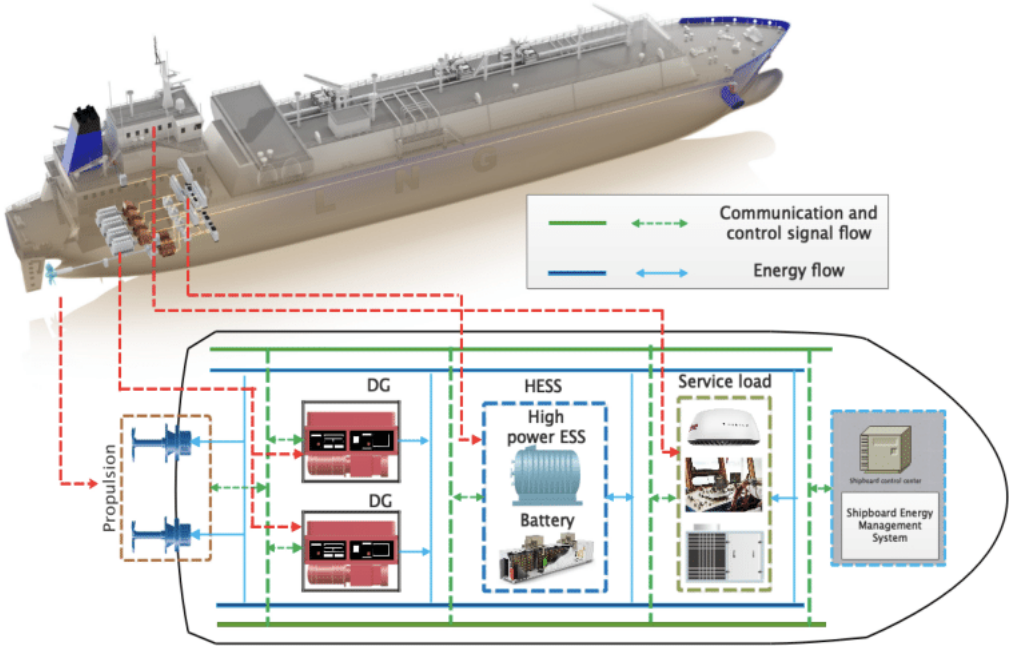

Figure 1.5: Topology of shipboard microgrid [19]

IPSs cane be categorized as either DC SMGs or AC SMGs according to the type of distribution system.
AC SMGs can actually be traced back to 1986, when a full electrical propulsion system was first installed onboard Queen Elizabeth II. During the following decades, more and more ships which relied on AC SMG and started sailing, which makes AC SMG the mainstream type of existing SPSs [20].

1.5.3 Land microgrids

Some of the most interesting recent MGs that have been realized is the Siemens Campus Microgrid, completed in 2020, which is a smart system to optimize energy management

and heating requirements on the company premises. “A smart microgrid controller centrally orchestrates the connected assets and optimizes the power supply to take account of peak loads and grid capacity utilization. That’s in addition to other influencing factors that result from independent generation,” says Werner Brandauer, Digital Grid, Siemens Smart Infrastructure [21].

On the other side of the equator, In 2017, ABB built a MG to supply the entire Robben island with solar power for at least nine months of the year, and eventually reducing the island’s CO2 emissions by 75%.

The MG of the Robben island consists of a photovoltaic system with a rated output of 667 kW, equipped with a battery storage system that has a capacity of 837 kWh.
An additional 500 kW, diesel-fired power plant ensures reliable supply even when the sky is cloudy and the batteries are drained. The complete system is monitored and controlled from Cape Town. Thanks to the MG, it is no longer necessary to have a service team for the grid permanently stationed on the island [22].

On the 9th of February, 2021, PT ABB Power Grids Indonesia, successfully deployed the first MG solution in Indonesia to ensure a continuous power supply for off-grid mining operations in Bontang, East Kalimantan. This MG is based on several PV systems, with the aim of reducing ITM’s carbon footprint – which is a key milestone in their commitment to reduce carbon emission, all while reducing operational cost as well.

Figure 1.6: Hitachi ABB Grids Indonesia [23]

Since it first started operating in 2019, the project has successfully integrated solar generation into the network,while ensuring stable and efficient energy supply to the customer. The system is expected to produce 230 MWh from solar PV annually [23].

1.6 Hierarchical control of AC microgrids

According to the IEEE Standard P2030.7 (Standard for the Specification of MG Controllers), the two core control functions for MG controllers are transition and dispatch. These two functions enable the MG to operate as a system that can manage itself— autonomously or with the grid—and connect or disconnect from the distribution grid.

We distinguish three main control levels to ensure a reliable and stable operation of an AC MG, which will be the MG architecture used in this project.

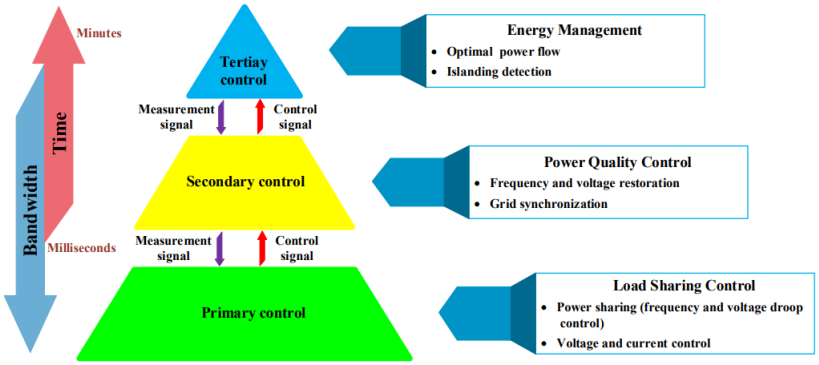

Figure 1.7: Hierarchical control structure of an MG

1.6.1 Primary control

The first level of the MG hierarchical control is the primary control or load-sharing level. As the name suggests, this level is responsible on providing appropriate real and reactive power sharing between the DGs by regulating the inverter voltage and frequency through voltage and current controller.
The primary current control approach is mainly divided into two types: linear current controller and non-linear current controller.
Linear current controller includes synchronous and stationary reference frame-based PI and PR regulator, feedback controller, adaptive, predictive, dead-beat regulator [24].
In the case of dc-input, the PI regulator is preferred thanks to its zero steady-state error. For ac-input, the PR regulator is selected thanks to the fast response [25].

On the other hand,linear regulator include hysteresis, SMC, wavelet, signal processing, fuzzy techniques, and ANN techniques.

a)Traditional droop approach

Traditional droop approach or TDA for short, is the same as PF/QV Droop approach. P-F DA is used to reduce the frequency of voltage output by increasing the real power generation.
Q-V DA, on the other hand, is used to reduce the magnitude of the output voltage by increasing the reactive power injection in the MG.

Put simply, TDA is used to mimic the machine inertia for regulating the mismatch in energy production and user demand by normalizing the frequency [26].

In the droop control loop, the frequency ω and the amplitude E of the inverter voltage output are fixed according to the average active power P, and the average reactive Q that are provided by the VSI to the MG. Their relation can be expressed as:

$$\omega = \omega_n - m \times (P^* - P) \tag{1.1}$$

$$E = E_n - n \times (Q^* - Q) \tag{1.2}$$

ω_n and En are the frequency and the amplitude of no-load output voltage, respectively. P and Q are the active and reactive power references, which are set to zero in the case of island operation mode.

The control parameters n and m correspond to the slopes of the frequency and amplitude functions, and can be determined according to the allowed frequency and voltage deviation $\Delta\ \omega$ and ΔE) and the maximum active and reactive powers (P_{max} and Q_{max}, respectively.

This relationship can be given as follows:

$$m = \frac{\Delta\omega}{P_{max}} \tag{1.3}$$

$$n = \frac{\Delta E}{Q_{max}} \tag{1.4}$$

The figure below shows the power sharing using droop control using TDA.

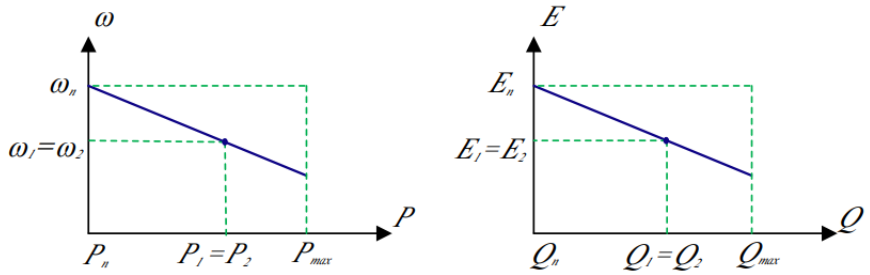

Figure 1.8: Active and reactive power sharing using droop control

b) Advanced droop approach

1. Phase Angle Droop Approach:

   A novel PADA method is proposed in references [27] and [28] to regulate the phase angle of the DG voltage sources with a common time reference. Thanks to that, the desired power can be fulfilled between the DGs, similar to TDA, by decreasing the magnitude and angle of the voltage.

$$\delta_n = \delta_r - M_p \times (P_n - P_{nr}) \tag{1.5}$$

$$E_n = E_r - N_q \times (Q_n - Q_{nr}) \tag{1.6}$$

2. VP - FQ approach:

   In an attempt to overcome the shortcomings of the TDA approach, a different V-P/F-Q based ADA is proposed for ow-voltage and high resistive distributed line application.

   In this droop approach, the output voltage magnitude is decreased with an improvement in real power while an increase in frequency is achieved with a boost in apparent power output. [29].

$$P = \frac{V_{inv} \times E - (V_{inv})^2}{z} \tag{1.7}$$

$$Q = -\frac{V_{inv} \times E\angle\delta}{z} \tag{1.8}$$

"Z" is the reactive impedance of the line. P-V decrease and F-Q increase characteristics are illustrated in the equations below:

$$V_n = V_r - D_t \times P \tag{1.9}$$

$$r.\omega_n = \omega_r + I_t \times Q \tag{1.10}$$

$$D_t = \frac{\Delta E}{P_m} \tag{1.11}$$

$$I_t = \frac{\Delta \omega}{2 \times Q_m} \tag{1.12}$$

3. Virtual output impedance loop approach:

   In order avoid the real and reactive power coupling, an advanced DA, the VIDA has been adopted.

   This method is designed by including the first control loop in the droop approach. The virtual fundamental impedance is used as a voltage feedback control loop.

   The output voltage of the inverter is regulated by modifying the value of the virtual output impedance, Z_v(s), [30]. The reference inverter output voltage, V_r, of the system is computed as follows:

$$V_r = V_\alpha - V_{dc} - Z_v(s) \times I_0 \tag{1.13}$$

   Where V_α denotes the fundamental voltage outcomes, the V_{dc} is the inverter's dc link voltage at no-load condition, and I_0 is the output current.

1.6.2 Secondary control

This control method is used to regulate the energy management system of the MG. SA is used to improve the power quality (PQ) by returning the voltage and frequency of the MG, as previously affected by the primary approach. In addition, this proposed approach also facilitated re-synchronization operation among the utility and DGs [31].

Centralized approach

In this structure, all the required parameters,i.e., the DG units' frequency and voltage, are generally transmitted via a high data rate communication bus. However, one of issues the centralized control structure suffers from the problem is the single point of failure [32].

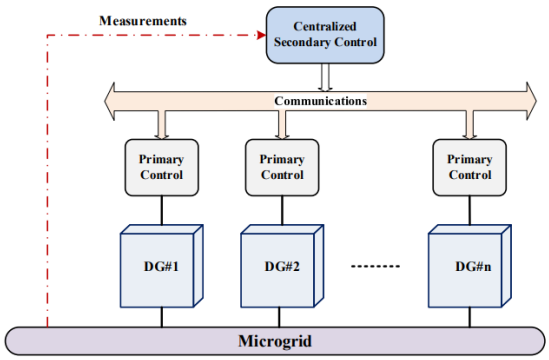

Figure 1.9: Control structure of centralized approach

Distributed approach

The distributed approach, unlike the centralized approach, is integrated at both the secondary and tertiary control levels for designing LV control and the main controller of the MG system.
The distributed approach facilitates communication among the MGs for better regulation, security, power quality, reliability, and intelligent control.
It is different from the centralized control approach as the local controllers are independent from each other, and operate according to the requirement [33].

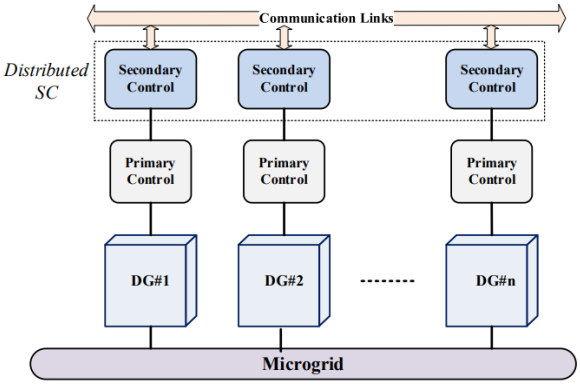

Figure 1.10: Control structure of distributed approach

Some of the most common distributed secondary control schemes are enumerated below.

1. Multi-agent approach:

   An agent that is physically/virtually present in the atmosphere is required to design the MAA controller.
   The agent is self-sufficient to react to any disturbances or changes in atmospheric conditions. In MAA, an agent's capability is estimated by its reaction to any change in atmospheric condition, pro-activeness, and communication with other agents.
   In Reference [34], a multiagent based hybrid energy managements for MG application is suggested, where more details about the approach are presented for further reading.

2. Model Predictive Approach:

   MPA consists of an objective function and a model of the process being controlled. The control includes physical and dynamic constraints which, together with the objective function, are used to perform an online optimization of the overall system[35].
   It is used to solve the optimization problem by appropriately forecasting the generation and load demand.
   By using the feedback control and regulating the power system constraints, the proposed MPA is applied to resolve the multi-variable evolution problem [36].

1.6.3 Tertiary control

The tertiary control layer, which is also the last layer in the hierachical control of MGs, is designed to regulate the active and reactive power flow between the main grid and the entire MG at the point of common coupling, PCC and ensure load balancing [37].

In the grid-connected mode, the MG operates by exporting and importing energy to and from the main grid, ensuring the power control flow balance between the MG and the main grid, and supporting the grid services as well.

To this end, the tertiary control is introduced as a global central controller for optimal bidirectional control of the active and reactive power flow, power management, and coordination of DG units at optimal set points [38].

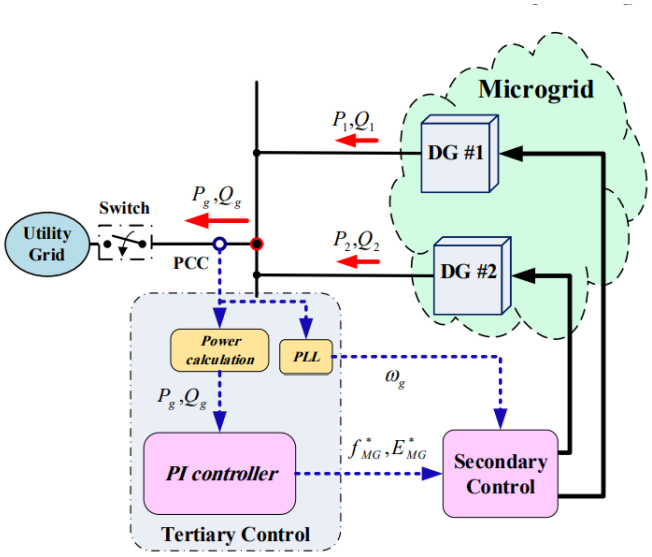

Figure 1.11: Tertiary control level schematic

1.7 Conclusion

In this chapter, an overall introduction to microgrids technology was presented, followed by the classifications of MGs. In addition to that, the hierarchical control of MGs and different control schemes used at each level were discussed. Various types of MG applications have been presented with the purpose of demonstrating the necessity of MGs and their vast areas of use.

Chapter 2

Voltage and Current control

2.1 Introduction

The primary control level of MGs is crucial in ensuring the smooth operation of the DGs. This present work aims to ensure a proper power-sharing between DGs of an AC MG. The proposed system is the design of a droop-controller proposed power sharing control scheme for an AC islanded microgrid. It consists in employing the droop-control strategy to ensure the power sharing between the DGs.
PI controllers are used to regulate the voltage and current of the VSIs to ensure stable and robust operation of the microgrid.

2.2 Proposed system

The AC MG is modeled as two parallel VSIs connected to a common load at the PCC.
The power-sharing scheme is composed of 4 main stages.

1. Parameter estimation
2. Power calculation
3. Power sharing
4. Current and voltage control

2.2.1 Parameter estimation

The conventional PLL schemes used for parameters' estimation in single phase systems are highly sensitive to load variation and harmonics issues. Another issue that affects their efficiency is the DC component disturbance [39].

This effect may significantly affect the performance of the frequency and amplitude restoration control loops. As a result, it will substantially decrease the entire MG system stability. Furthermore, as the PLL involves sine and cosine functions, which suffer from implementation complexity, it becomes hard to actually implement, especially, in the case of single-phase systems.
This issue may further complicate the implementation of secondary control and increase its computational time.

In addition to that, the DC component, which may be induced in the input of the PLL, can affect the PLL's estimation performance greatly and, hence, the system stability.
To deal with the PLL's issues, a number of advances solutions has been proposed in the literature with the capability of DC-offset rejection [40].
One of the proposed PLLs is SOGI-PLL, which was chosen for the parameter estimation in this system.

The schematic diagram of SOGI-PLL can be seen in the figure below:

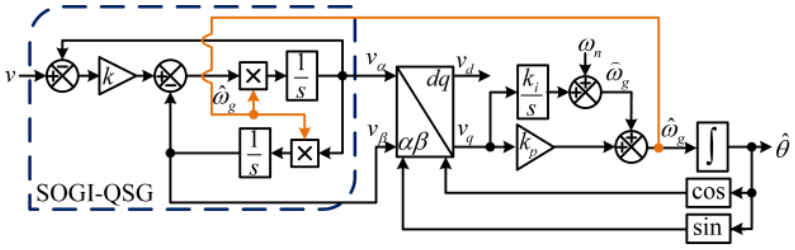

Figure 2.1: Structure of SOGI-PLL

SOGI structures are essentially notch filters (band-pass) that can be easily tuned to the grid frequency to ensure synchronisation.
They have been receiving a growing interest in the research community as they have the benefit of providing simultaneous access to both the filtered output as well as quadrature-shifted version of the same output (α and β axes).
Hence, allowing an easy implementation that can fit that of conventional dq-type PLLs (using the Park transform as phase detector).

2.2.2 Power calculation

The power calculation block is introduced into the primary control scheme in order to calculate the average value of the active and reactive powers of each DG unit.

The instantaneous active and reactive powers can be computed based on their mathematical expressions either in α β frame or dq frame as a function of output voltage and current α β (or dq) components, by using the well-known expressions given below:

$$P = 1/2(Vc\alpha \times I_\alpha + Vc\beta \times I_\beta) \tag{2.1}$$

$$Q = 1/2(Vc\alpha \times I_\alpha - Vc\beta \times I_\beta) \tag{2.2}$$

The following pair of equations can also be used in case the dq-frame components are used instead:

$$P = 1/2(Vcd \times I_d + Vcq \times I_q) \tag{2.3}$$

$$Q = 1/2(Vcd \times I_q + Vcq \times I_d) \tag{2.4}$$

Where $V_{c\alpha\beta}$ and $I_{c\alpha\beta}$ are the in-phase ad quadrature inverter output voltage and current, respectively.

After the instantaneous active and reactive powers are calculated, they are passed through a low-pass filter (LPF) in order to obtain the corresponding average values.
The LPF transfer function can be expressed in the s-domain.

$$G_{LPF}(s) = \frac{P}{p} = \frac{\omega_{cut-off}}{s + \omega_{cut-off}} \tag{2.5}$$

$\omega_{cut-off}$ denotes the cut-off frequency of the LPF which is generally chosen with a very small value to eliminate the inherent harmonics components. The calculated active and reactive power are then sent as inputs to the droop controller [41].

2.2.3 Power sharing

In order to ensure appropriate power sharing between different DGs of the MG, the droop-control strategy has been adopted.

It ensures that all the DG units of the system share the load by drooping the frequency of each VSI with the delivered real power.
This operation allows each generator to share changes in total load in a way that is determined by its own frequency droop characteristic, without the need for a communication link with the other DG units.

Similarly, a drop in the voltage amplitude (E), that depends on the reactive power (Q) of the DG is used in order to ensure proper reactive power-sharing in the MG [42].

The active and reactive power sharing can be achieved by adjusting the values of the frequency and voltage, respectively. This adjustment can be expressed by the equations 1.1 and 1.2 seen previously in the section 1.4.1. For the sake of reminder, the equations are provided below:

$$\omega = \omega_n - m \times (P^* - P) \tag{2.6}$$

$$E = E_n - n \times (Q^* - Q) \tag{2.7}$$

ω_n and E_n are the frequency and the amplitude of no-load output voltage, respectively. P and Q are the active and reactive powers, respectively. n and m, which are the control parameters, n and m correspond to the slopes of the frequency and amplitude functions depend on the allowed frequency and voltage deviation (ω and Δ E) and the maximum active and reactive powers (P_{max} and Q_{max}), respectively. This relationship, previously covered in the section 1.6.1, can be given as follows:

$$m = \frac{\Delta\omega}{P_{max}} \tag{2.8}$$

$$n = \frac{\Delta E}{Q_{max}} \tag{2.9}$$

In our system, the values used for the control parameters are m = 0.001 rad/W.S and n = 0.0003 V/VAR. Figure 3.32 shows that the produced frequency and voltage by the droop controller are entered into a sinusoidal signal generator to generate the reference of the output voltage of the VSI.

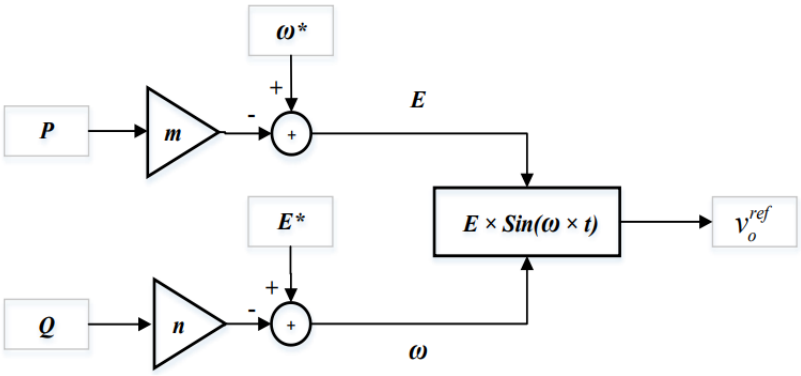

Figure 2.2: Power sharing control diagram

With $E^* = 310$ V and $\omega^* = 314$ rad/s, which are the reference values of the grid. The reference of the VSI's output voltage is defined by the equation:

$$v_0^*(s) = E \times sin(\omega t) \tag{2.10}$$

This determined voltage reference by the droop control is then applied to the input of the inner voltage and current control loops.

2.2.4 Inner voltage and current control loops

The inner controllers are required to maintain stable control over the output voltage and current of the inverter, even in the presence of disturbances.
This goal can be achieved by setting the output voltage of the inverter to the desired reference. The inner controller that is considered for VSIs includes a voltage loop and an inner current loop.
The current and voltage control loops are performed to regulate the output voltage of the inverter and to control the current while maintaining the system stable.

The closed-loop transfer function of the inverter output-voltage can be obtained using the following expression:

$$v_o = G_v(s) v_{oN}^{ref} \tag{2.11}$$

Where s is the Laplace operator, v_{oN}^{ref} is the output-voltage reference comes from the droop control. G(s) is the voltage gain, which can be expressed as:

$$G_v(s) = \frac{\frac{k_{i-v}k_{i-i}}{C_f L_f}}{s^4 + \frac{R_f + k_{p-i}}{C_f L_f} s^3 + \frac{k_{i-i}}{C_f L_f} s^2 + \frac{k_{i-i}k_{p-v}}{C_f L_f} s + \frac{k_{i-i}k_{i-v}}{C_f L_f}} \tag{2.12}$$

L_f and C_f are the inverter's LC filter parameters, and k_{i-v}, k_{p-i}, k_{i-i} and k_{p-v} are the PI controller gains.
The values of the gains were determined by tuning, trial and error method.
The final values used in our design can be summarized in the table below:

k_{p-v}	k_{i-v}	k_{p-i}	k_{i-i}
0.311	7	27.06	0.567

Table 2.1: PI controller parameters

2.3 Conclusion

This chapter has covered the proposed primary control for an AC MG in its islanded operation. The controller is required to achieve proper power balance between different DGs of the system while keeping a stable voltage and frequency under different scenarios.
The different stages of the primary control level were detailed, along with the equations and expressions used for parameter calculation.

Chapter 3

Simulation and results

In order to test the proposed system and simulate the MG, Simulink was used to carry out the simulation of the MG controller.
Figure 3.1, in the next page, shows the Simulink model of the AC MG and the architecture of the droop-based power-sharing controller. N.B. The PLL initial frequency was set to 50 Hz in the Simulink block as this was the only value that ensures fast convergence.

3.1 Simulink model

3.1.1 Proposed system

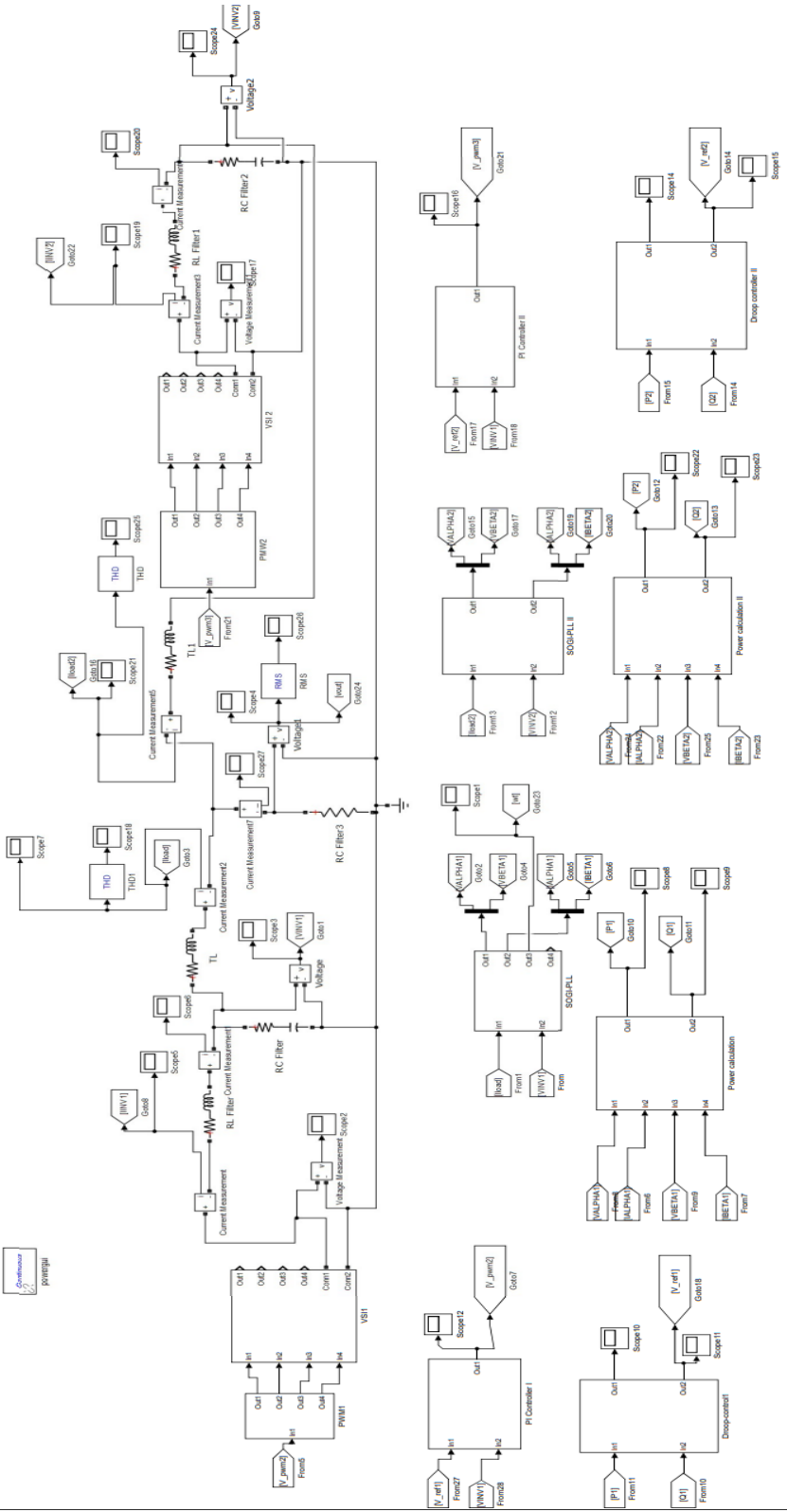

Figure 3.1: Simulink model of the proposed system

3.1.2 droop-control

The main component of the power-sharing scheme is the droop-controller. The sub-system of its Simulink model can be seen in the figure below:

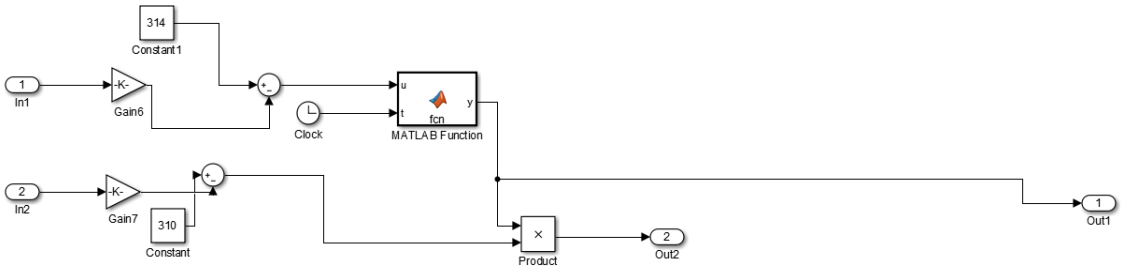

Figure 3.2: Simulink model of the droop-control block

Where input 1 and input 2 are the active and reactive powers, respectively. The reference voltage that is sent to the PI controller is the signal out 2.

3.1.3 PI controller

The inner voltage and current controller was implemented using a PI controller, detailed in the next figure:

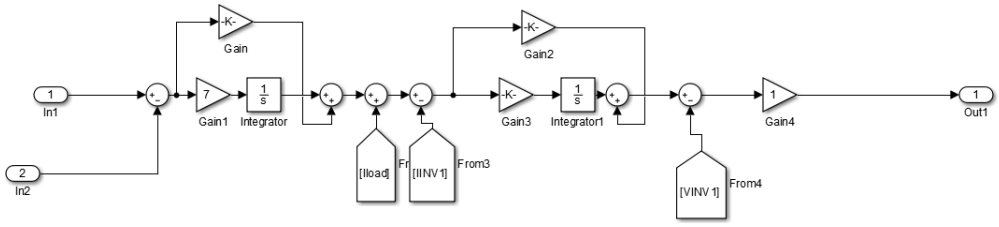

Figure 3.3: Simulink model of the PI controller

Where input 1 and input 2 are the reference voltage, which is the output of the droop-controller, and the inverter filtered voltage, respectively.

3.2 Output of different scenarios

In order to assess the effectiveness of the system, it has to be tested under different scenarios to ensure a proper functioning regardless of the load and generation condition.
A proper controller must maintain constant and stable voltage and frequency in the MG under all conditions.

3.2.1 Resistive load

The system was first tested with a regular resistive load of 1000 Ω. The different measured characteristics are illustrated in the following sections.

Output voltage

The figures below show the measured voltage at the PCC.

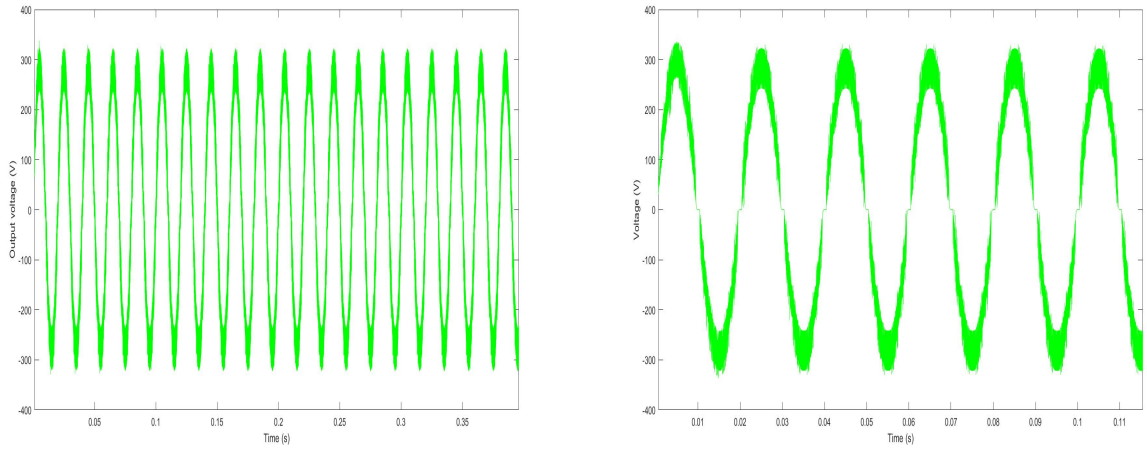

Figure 3.4: Output voltage at PCC - Case of resistive load

Output current

The output current measured at the PCC can be seen in the waveforms that follow.

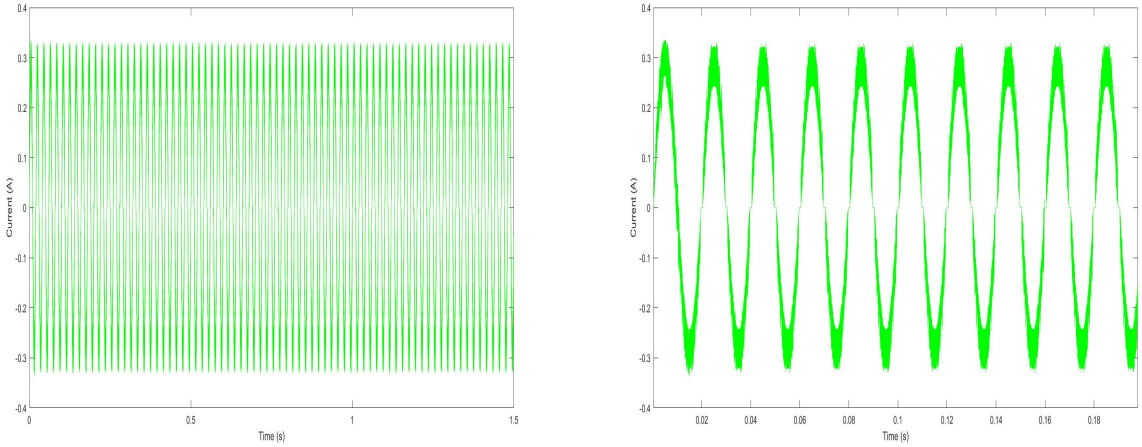

Figure 3.5: Output current at PCC - Case of resistive load

Output voltage of the VSIs

Since the MG system studied is AC, an inverter must be added to each DC DG. The raw output of VSI1 can be seen in the following graphs.

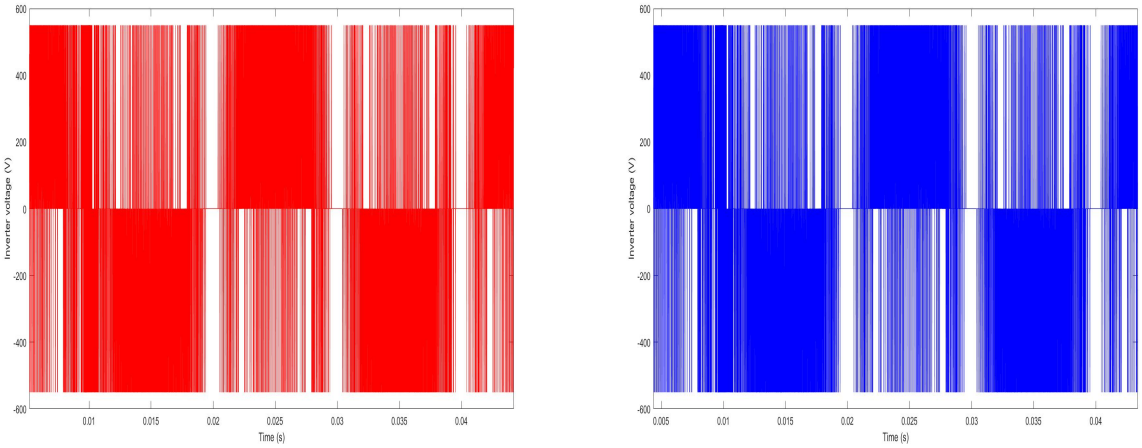

Figure 3.6: Output voltage of VSIs - Case of resistive load

The output voltage of the VSIs is filtered using an LC filter. The resulting output voltage is illustrated in the figures below.

Filtered output voltage of VSI 1

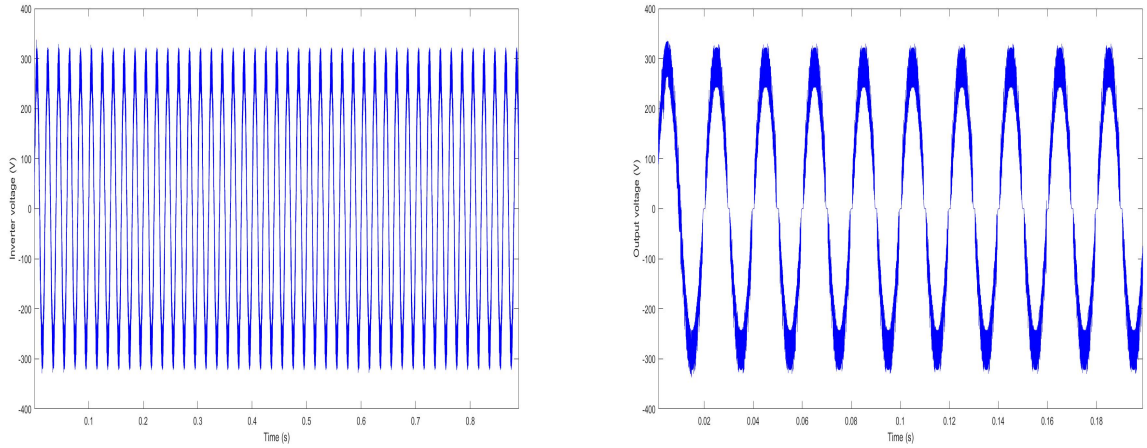

Figure 3.7: Filtered output voltage of VSI 1

Filtered output voltage of VSI 2

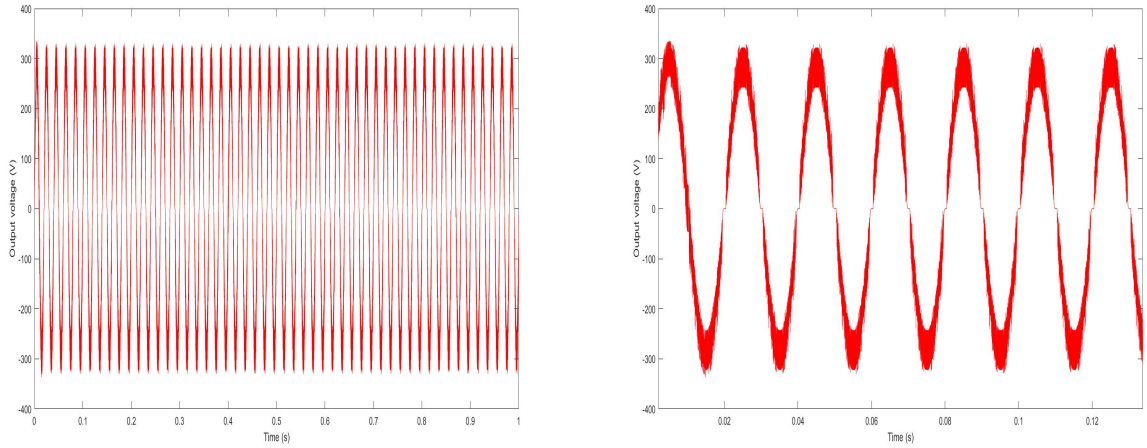

Figure 3.8: Filtered output voltage of VSI 2

The current at the output of both inverters was measured to see the current sharing between different DGs of the MG.

Output current VSI 1

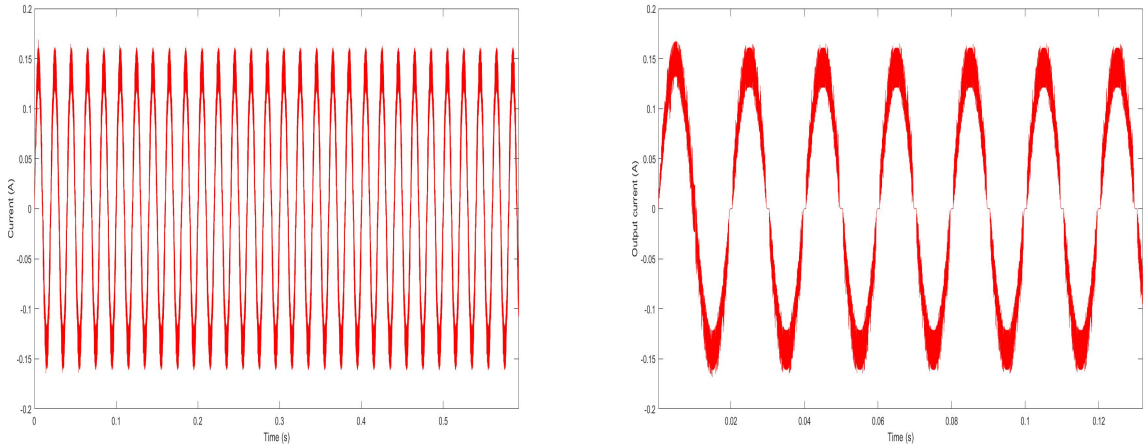

Figure 3.9: Filtered output current of VSI 1

Output current VSI 2

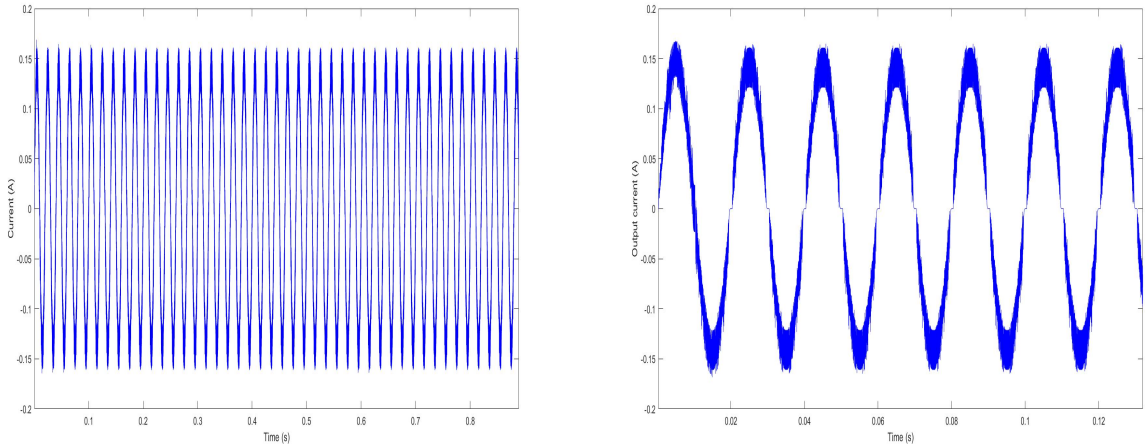

Figure 3.10: Filtered output current of VSI 2

Total Harmonic Distortion

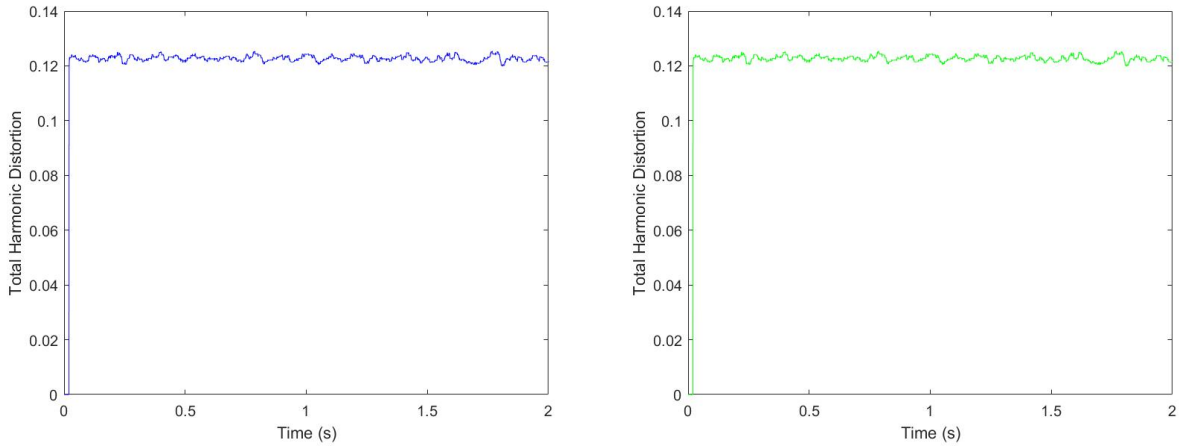

(a) THD of DG1 (b) THD of DG2

Figure 3.11: Total Harmonic Distortion of the MG

Active power

In order to assess the effectiveness of the controller, proper power sharing must be achieved between both DGs. In the figure below, the average active power of both DGs is measured.

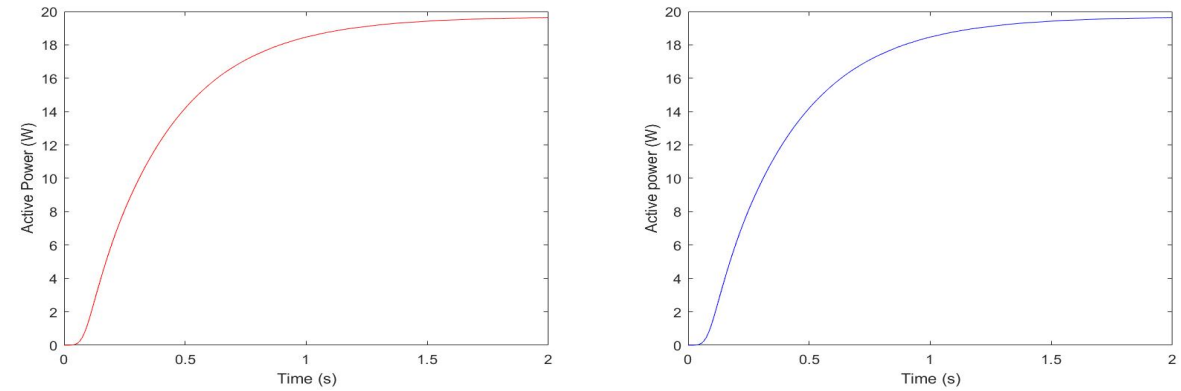

(a) Active power of DG1 (b) Active power of DG2

Figure 3.12: Active power of both DGs

Reactive power

In order to assess the effectiveness of the controller, proper power sharing must be achieved between both DGs. In the following figure, the average reactive power of both DGs is measured.

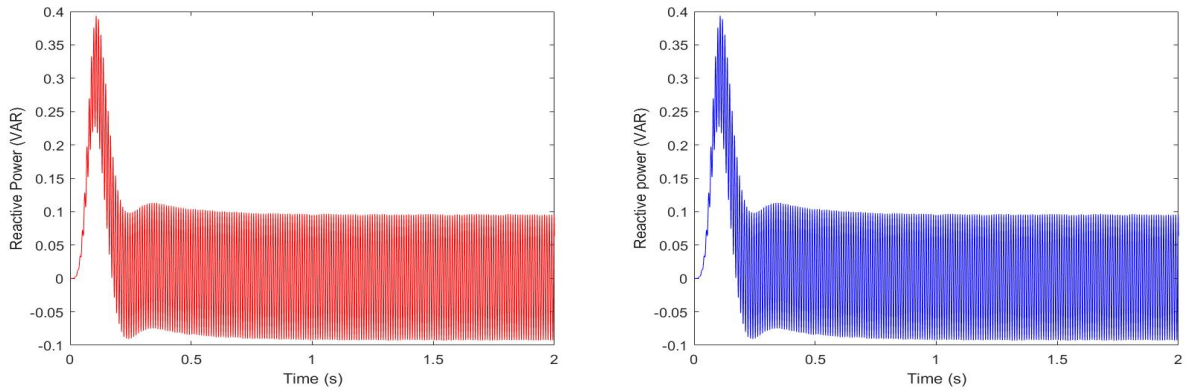

(a) Reactive power of DG1 (b) Reactive power of DG2

Figure 3.13: Reactive power of both DGs

Frequency

The frequency of the system was measured using SOGI-PLL. For the sake of comparison, conventional PLL was also used for frequency estimation. Both results are illustrated in the graphs below:

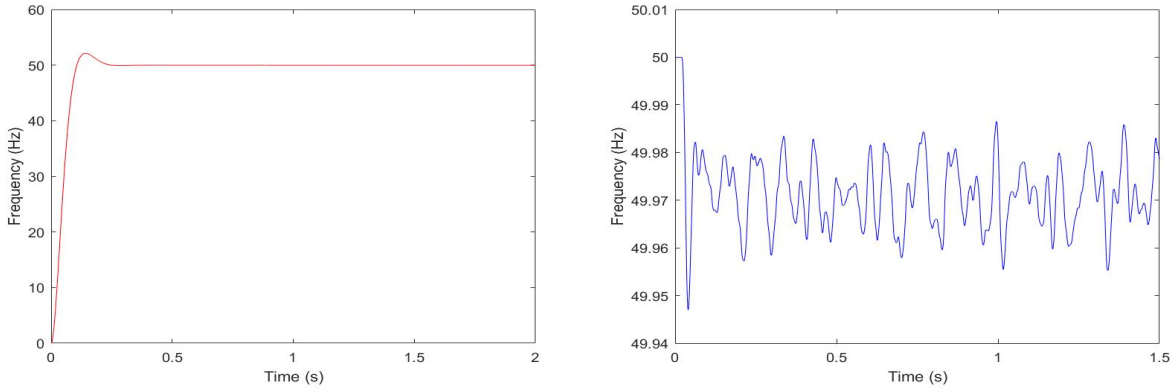

(a) Using SOGI-PLL (b) Using PLL

Figure 3.14: Frequency of the system

Discussion

From the resulting graphs of the first case: Resistive load, it is clear that the MG controller achieved its purpose. The voltage at the PCC and at each DG is equal to the nominal value, V_{peak} = 310 V, and the frequency is around 50 Hz. The PLL measured frequency shows that the deviation doesn't exceed 0.1 % which falls under the permitted standard variation, which is 1%. Furthermore, the power and reactive power are shared equally between both DFs, considering that they have similar characteristics. The THD is around 0.12% which is considerably below the allowed maximum values of 5%.

3.2.2 Inductive load

The second test that was performed on the system was under the case of feeding an inductive load. The obtained simulation results are illustrated in the following sections.

Output voltage

The output voltage at the PCC measurement can be seen in the graphs below.

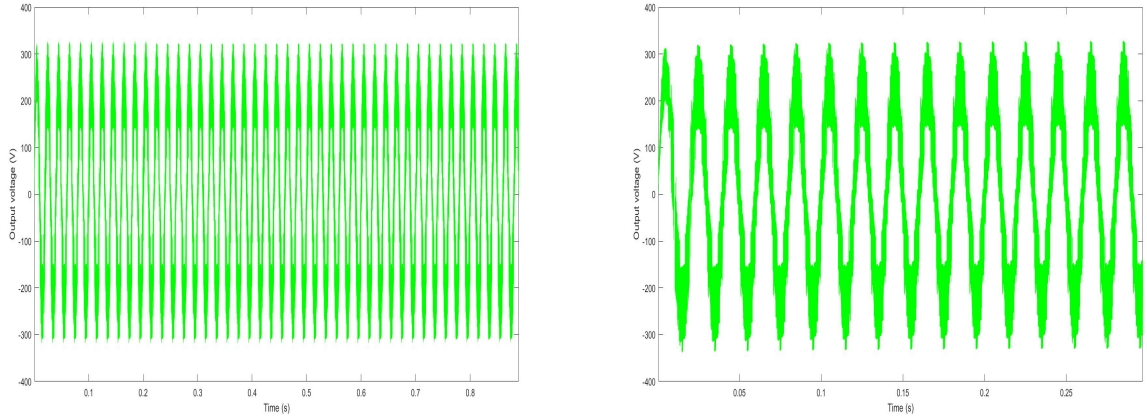

Figure 3.15: Output voltage at PCC - Case of inductive load

Output current

In addition to voltage, the current was also measured at PCC, giving the following resut=lts:

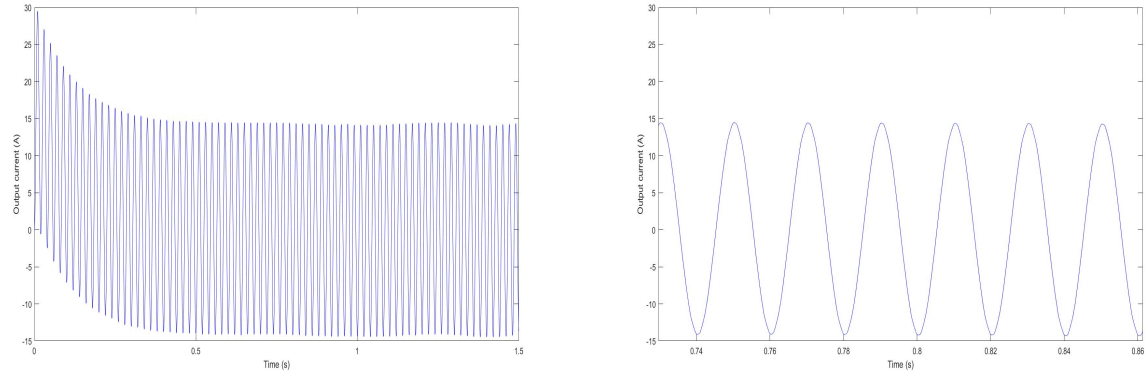

Figure 3.16: Output current at PCC - Case of inductive load

Output voltage of VSIs

The voltage of both inverters was measured, before the LC filtering

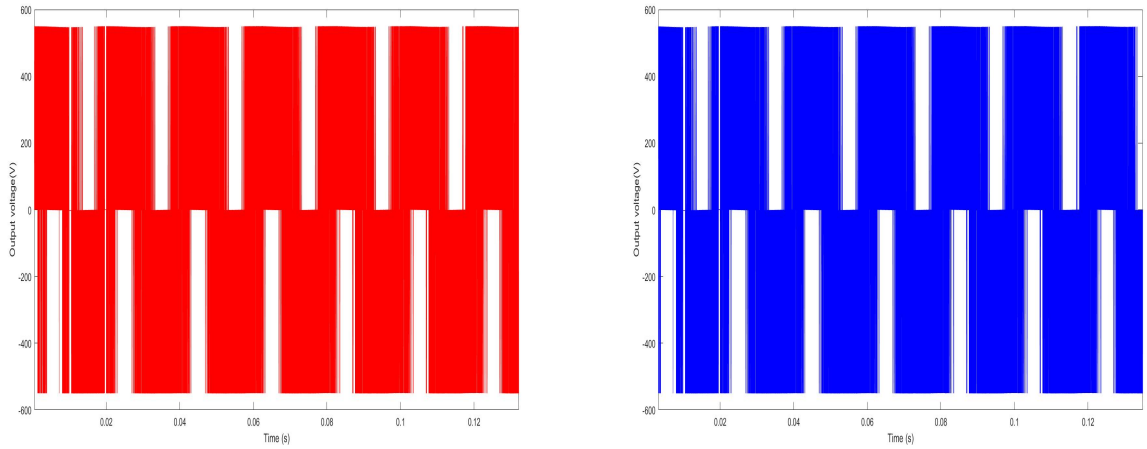

Figure 3.17: Output voltage of VSIs - Case of inductive load

The voltage after the LC filter is a sinewave. The filtered voltage was measured at the output of each filter. The results are as illustrated in the figures below.

Filtered output voltage of VSI 1

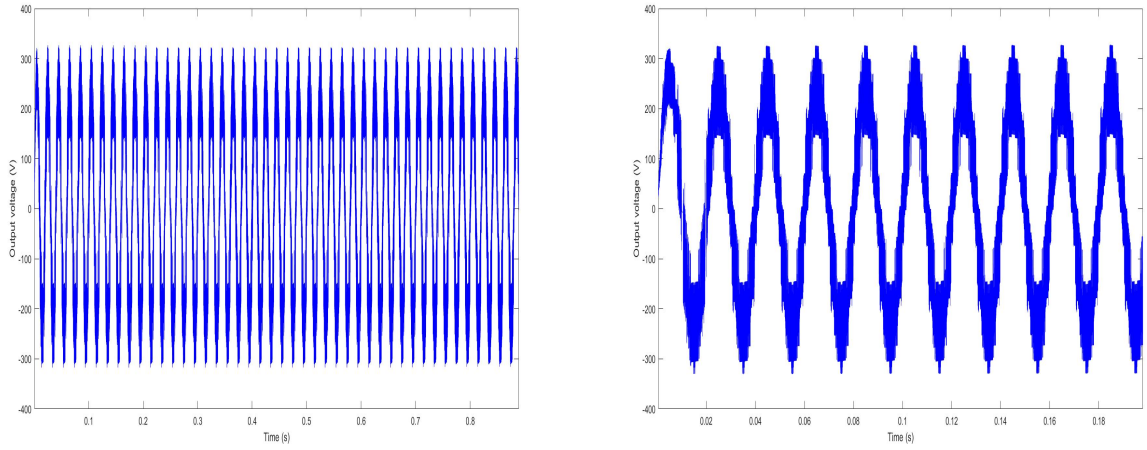

Figure 3.18: Filtered output voltage of VSI 1- Case of inductive load

Filtered output voltage of VSI 2

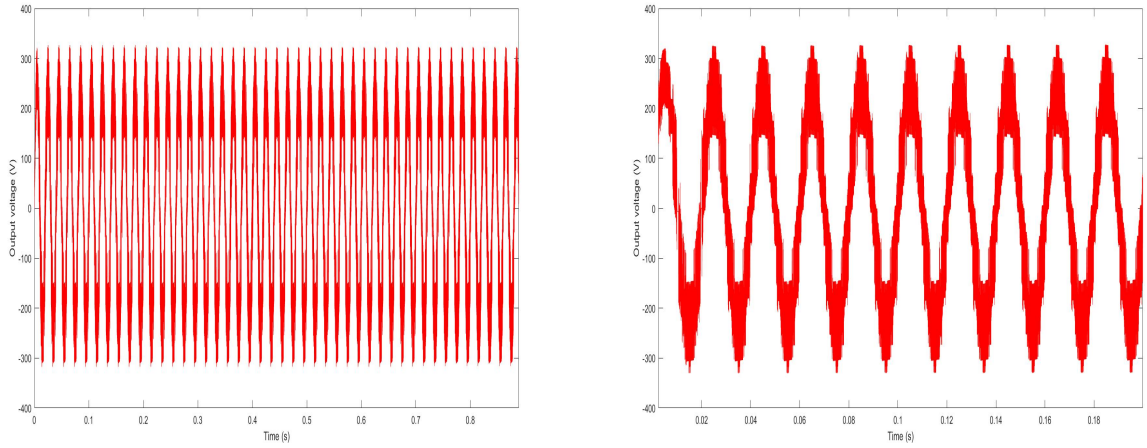

Figure 3.19: Filtered output voltage of VSI 2- Case of inductive load

The current at the output of each VSI was also measured, the resulting waveforms are shown below.

Current of VSI 1

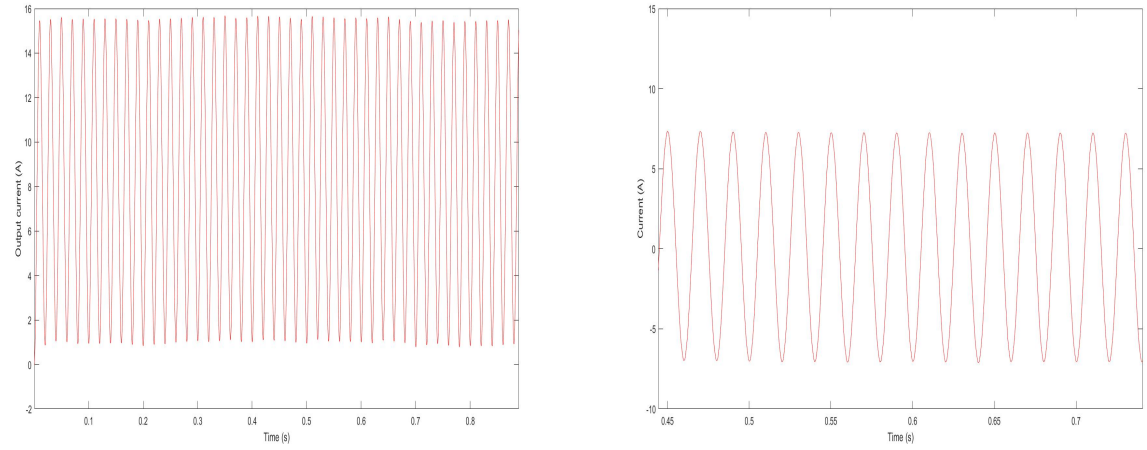

Figure 3.20: Filtered output voltage of VSI 1 - case of inductive load

Current of the VSI 2

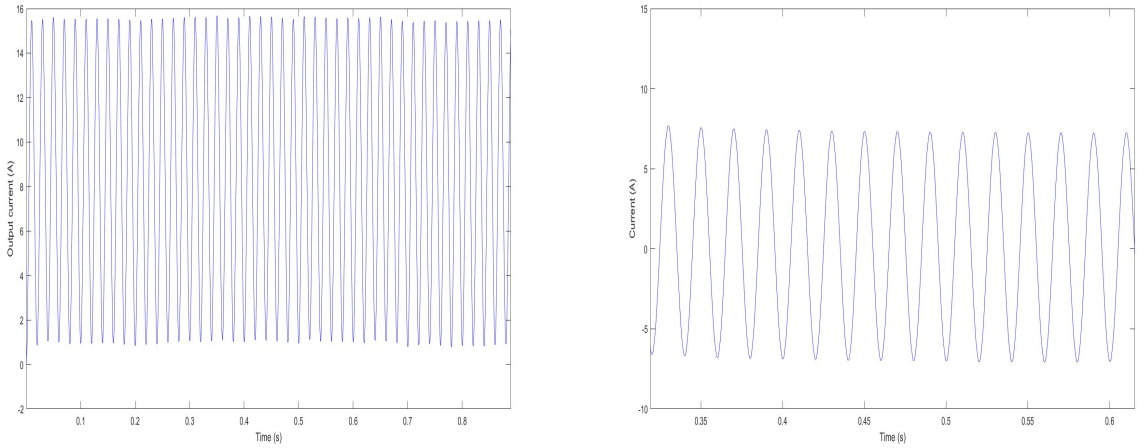

Figure 3.21: Filtered output voltage of VSI 2 - case of inductive load

Total Harmonic Distortion

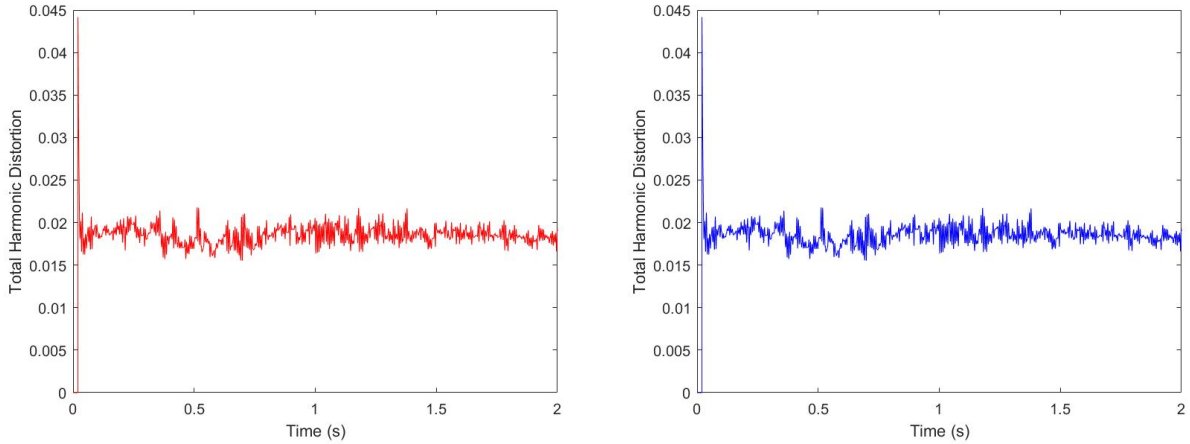

(a) THD of DG1 (b) THD of DG2

Figure 3.22: Total Harmonic Distortion of the MG - case of inductive load

Active power

The active power sharing can be seen in the figures below, where the average active power of each DG is illustrated.

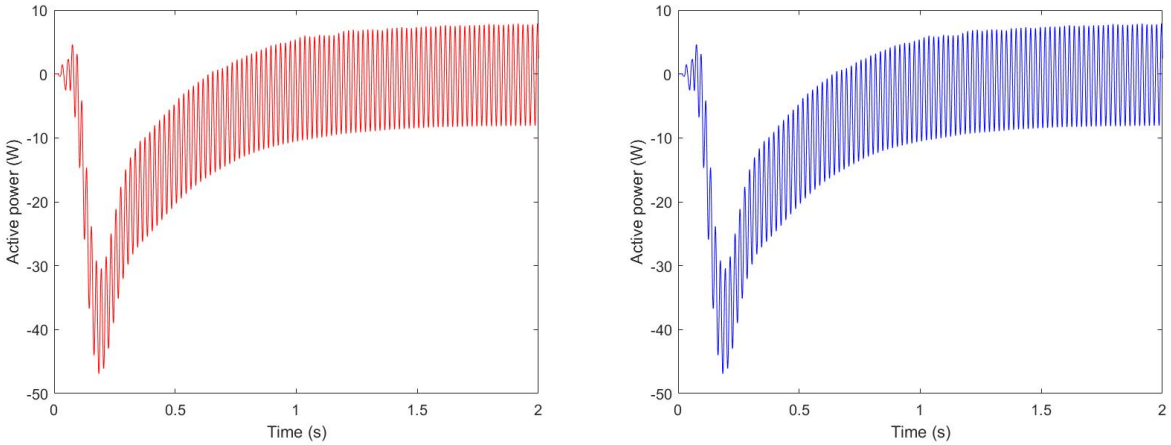

(a) Active power of DG1 (b) Active power of DG2

Figure 3.23: Active power of the MG - case of inductive load

Reactive power

The average reactive power of each DG is illustrated below.

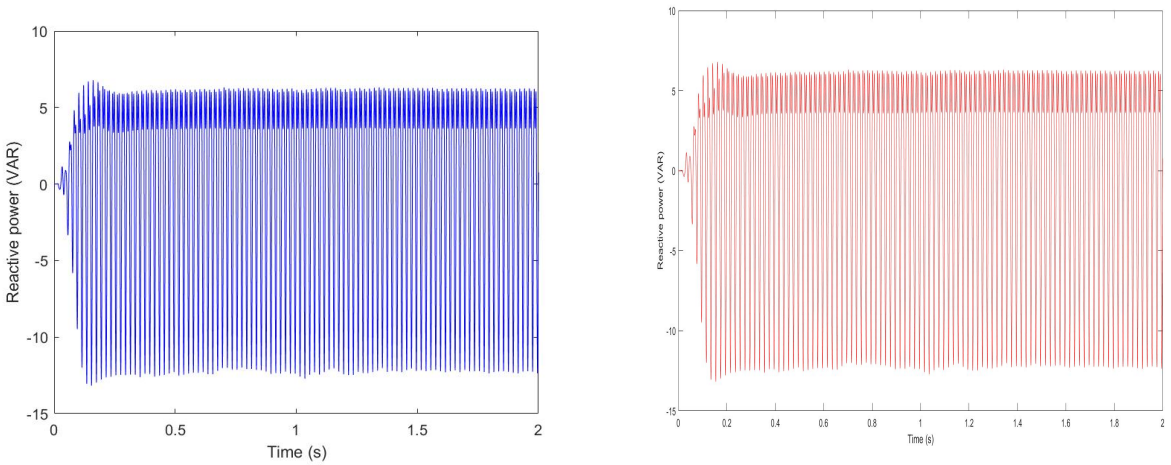

(a) Reactive power of DG1 (b) Reactive power of DG2

Figure 3.24: Reactive power of the MG - case of inductive load

Frequency

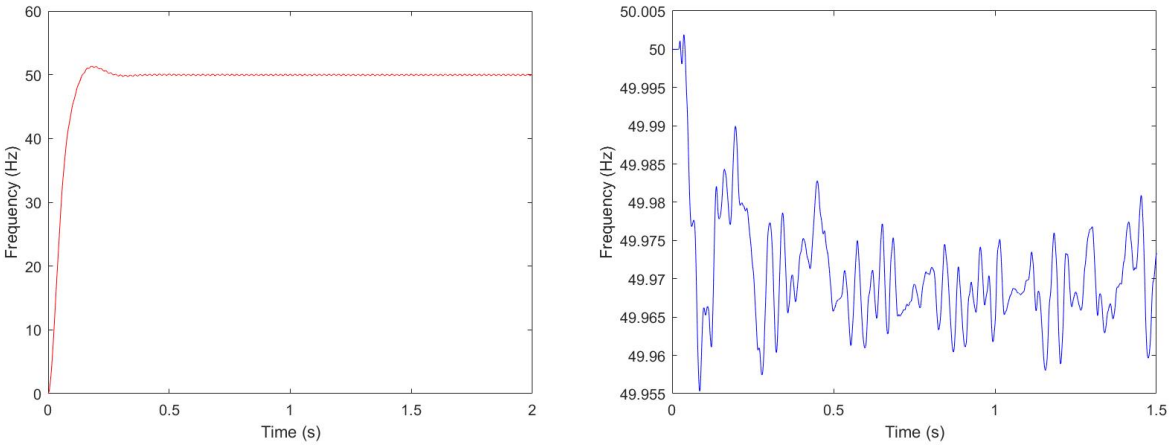

Figure 3.25: Frequency of the system - case of inductive load

Discussion

Some minor fluctuations can be noticed in the voltage and current waveforms, due to the inductive nature of the load. However, the voltage at the PCC and at each DG is equal to the nominal value, $V_{peak} = 310$ V, and the frequency is kept around 50 Hz with minor fluctuations.
The PLL measured frequency shows that the deviation doesn't exceed 0.1 % which falls under the permitted standard variation, which is 1%. Furthermore, the power and reactive power are shared equally between both DGs, considering that they have similar characteristics. The active power fluctuates around since the load is purely inductive. The THD is around 0.02% which is considerably below the allowed maximum values of 5%. After simulating the system with the MG feeding an inductive load, one can notice from the resulting graphs that under this load as well, the MG controller achieved its purpose.

3.2.3 Non-linear load

In order to assess the MG controller's functioning, the system must be tested under various conditions and load variations.
Since most real loads are non-linear, the third test was made with the MG feeding a non-linear load. The load used in the simulation was a half-wave rectifier with a forward diode voltage of $V_d = 0.8$ V.
The response of the system to feeding non-linear load is shown in the figures that follow.

Output voltage

The first voltage to be measured is the output voltage at the PCC, across the non-linear load. The test resulted in the graphs below.

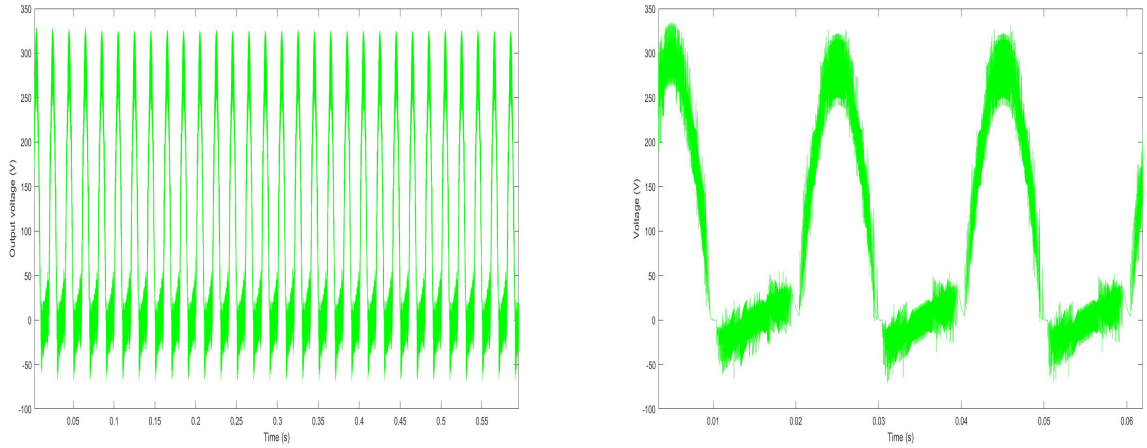

Figure 3.26: Ouput voltage at PCC - case of nonlinear load

Output current

The current at the PCC was also measured, which resulted in the following graphs:

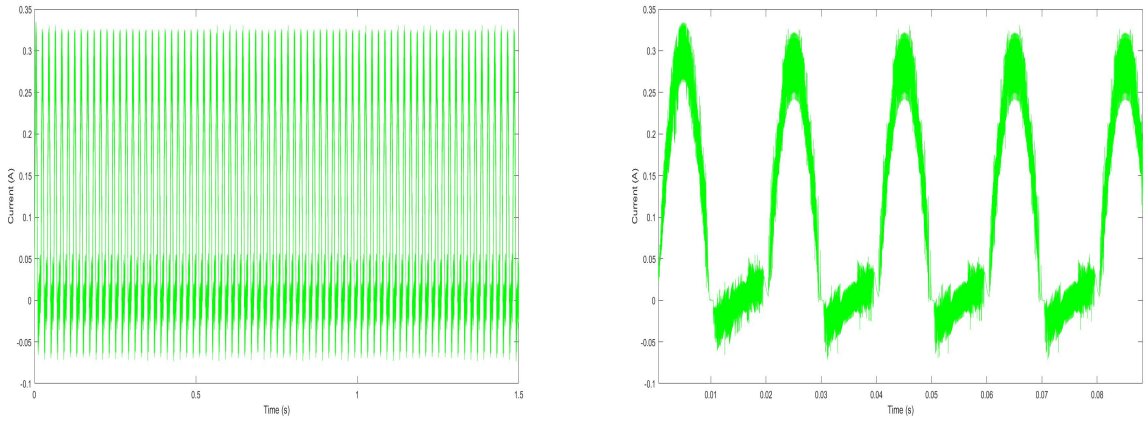

Figure 3.27: Ouput current at PCC - case of nonlinear load

The output of each inverter, before filtering, was measured. The resulting waveforms of both VSIs outputs is shown in the figures below.

Output voltage of VSIs

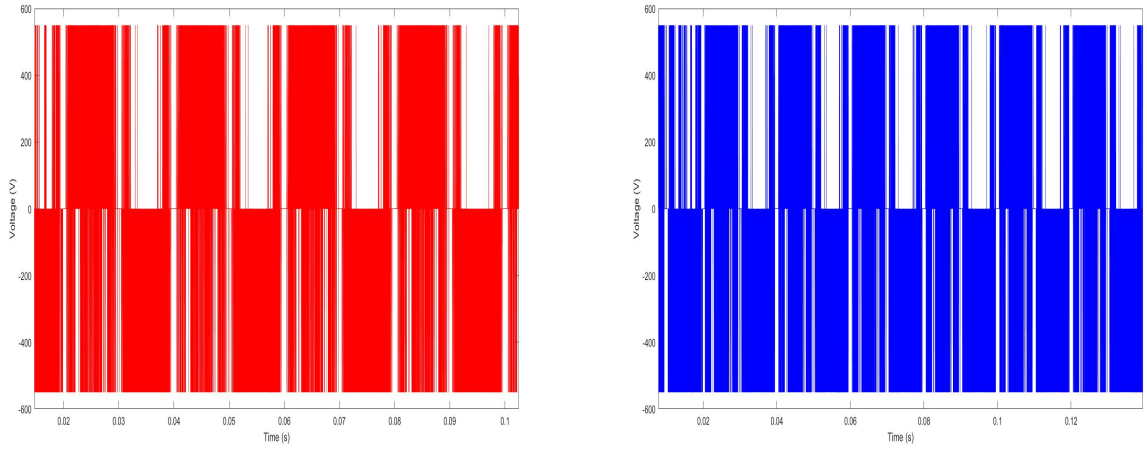

(a) Inverter voltage - VSI 1

(b) Inverter voltage - VSI 2

Figure 3.28: Inverter voltage - Case of non-linear load

The obtained inverter voltage post-filtering for each VSI is illustrated in the figures that follow.

Filtered output voltage - VSI 1

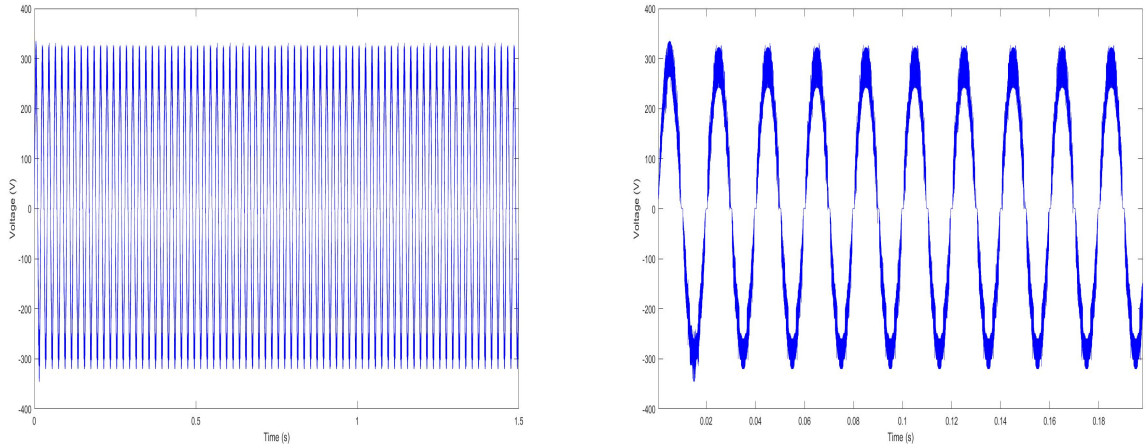

Figure 3.29: Filtered ouput voltage - VSI 1

Filtered output voltage - VSI 2

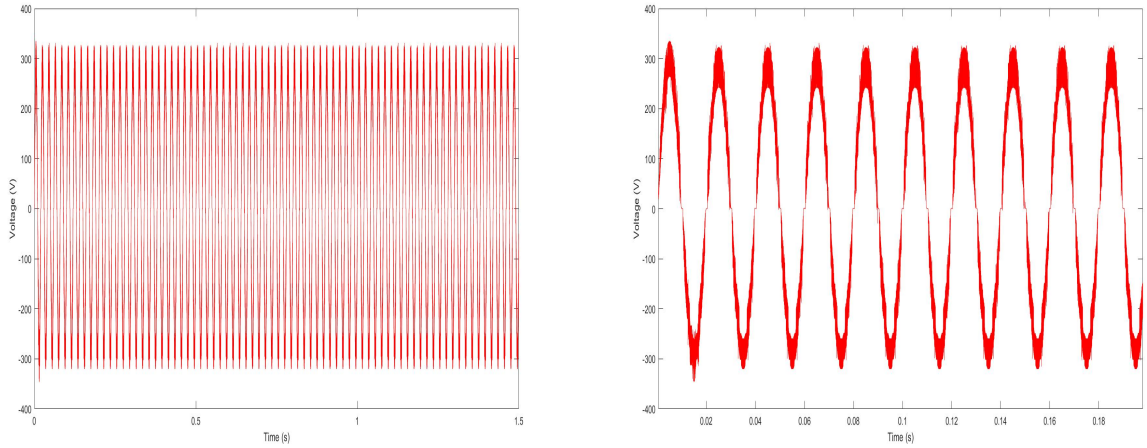

Figure 3.30: Filtered ouput voltage - VSI 2

In addition to inverter output voltage, the output current of each VSI was also measured, and the resulting graphs are displayed in the figures that follow.

Current of the VSI 1

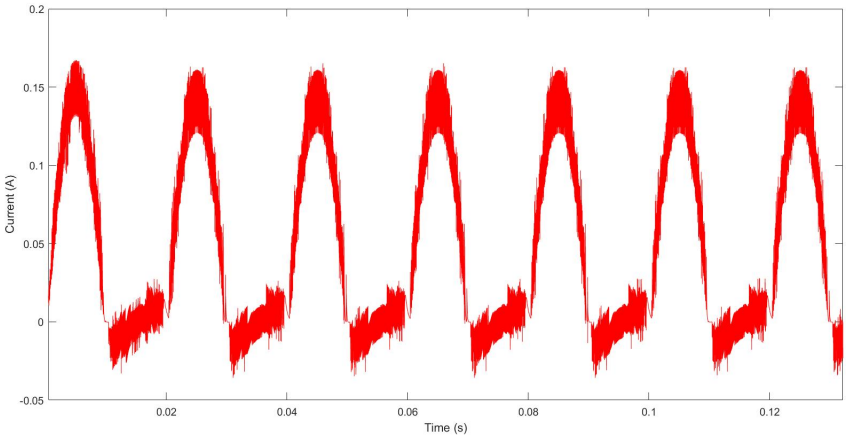

Figure 3.31: Output current produced by VSI 1

Current of the VSI 2

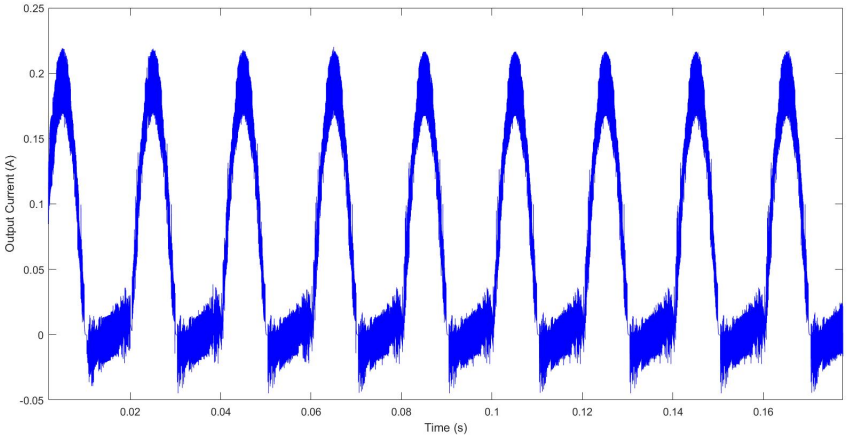

Figure 3.32: Output current produced by VSI 2

Total Harmonic Distortion

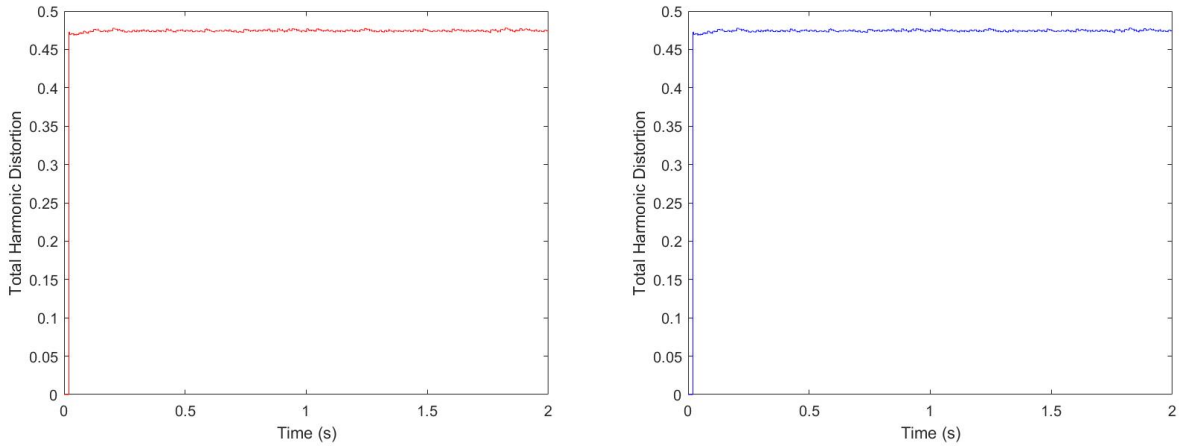

(a) THD of DG1 (b) THD of DG2

Figure 3.33: Total Harmonic Distortion of the MG

Active power

In order to assess the active power- sharing among DGs, active power of each DG of the MG was measured, resulting graphs are as follows.

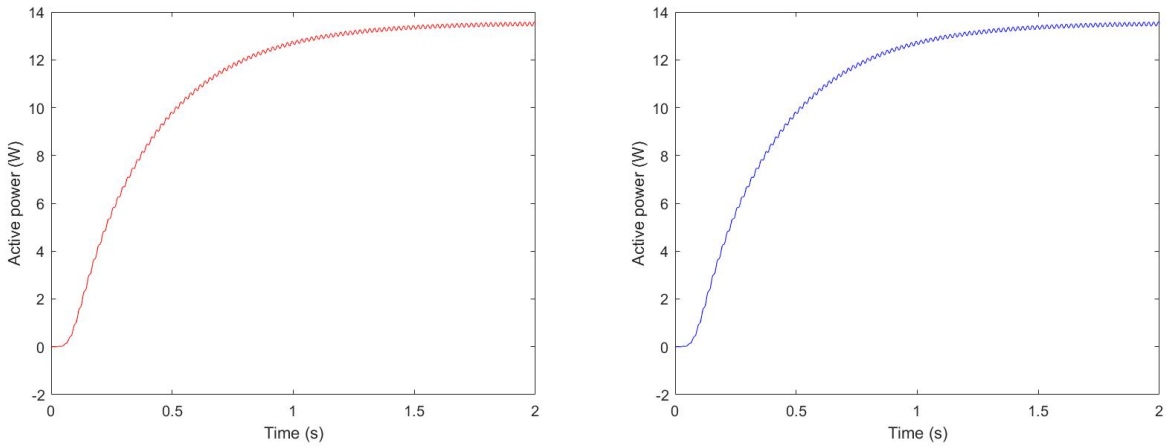

(a) Active power of DG1 (b) Active power of DG2

Figure 3.34: Active power of the MG

Reactive power

In order to assess the reactive power- sharing among DGs, reactive power of each DG of the MG was measured, resulting graphs are as follows.

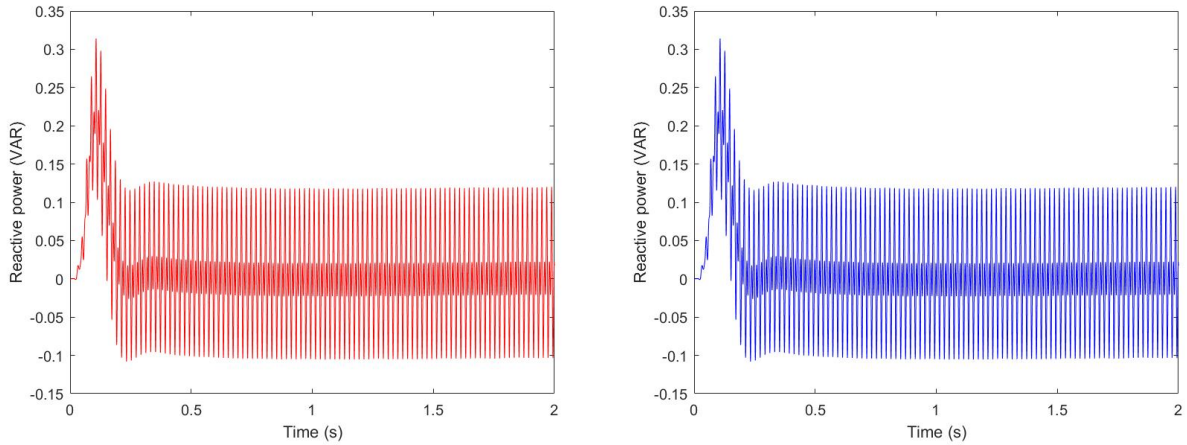

(a) Reactive power of DG1 (b) Reactive power of DG2

Figure 3.35: Reactive power of the MG

Frequency

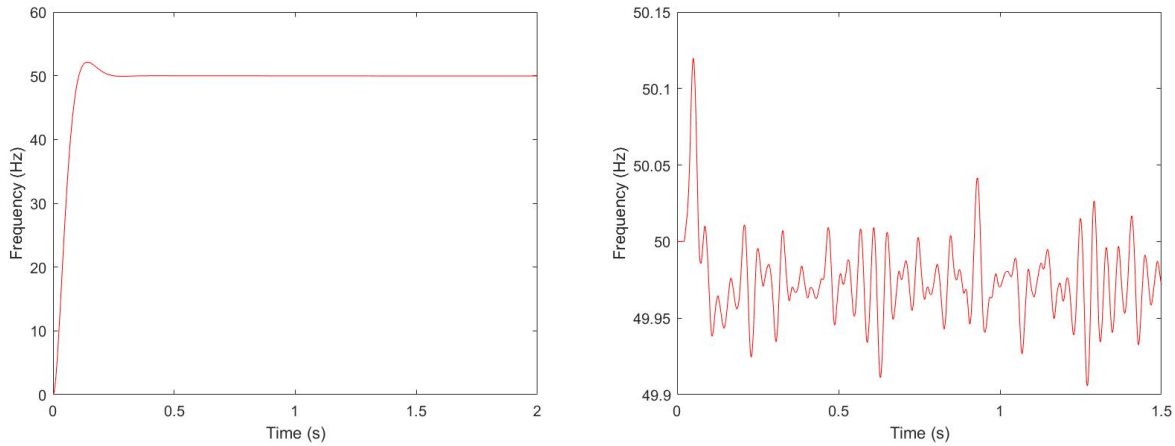

(a) Using SOGI-PLL (b) Using PLL

Figure 3.36: Frequency of the MG - case of nonlinear loads

Discussion

Some minor fluctuations can be noticed in the voltage and current waveforms, due to the non-linear nature of the load fed by the MG, in addition to a small DC offset, considering the fact that the non-linear load used is a HWR. However, the voltage at the PCC and at each DG is equal to the nominal value, $V_{peak} = 310$ V, and the frequency is kept around 50 Hz in the system.
The PLL measured frequency shows that the deviation doesn't exceed 0.1 % which falls under the permitted standard variation, which is 1%. A minor overshoot can be noticed at the beginning, in the transient state, that quickly fades. Furthermore, the power and reactive power are shared equally between both DGs, considering that they have similar characteristics. The reactive power fluctuates around since the load does not include any inductive elements. The THD is around 0.45% which is higher than the previous tests, but is still considerably below the allowed maximum values of 5%.

After simulating the system with the MG feeding an inductive load, one can notice from the resulting graphs that even under non-linear load well, the MG controller achieved its purpose, and that both THDs and active-power are properly shared between the DGs of the system.

3.2.4 Added loads

In addition to ensuring power sharing and stable voltage and frequency under different load conditions, the MG must also satisfy these conditions even in the case of disturbances. The first scenario the system was simulated under is the case of added loads. At time t=0.5s, an additional load is connected to the PCC.
The response of the MG is illustrated in the graphs that follow.

Output voltage

The resulting voltage at PCC during this scenario can be seen in the figures below.

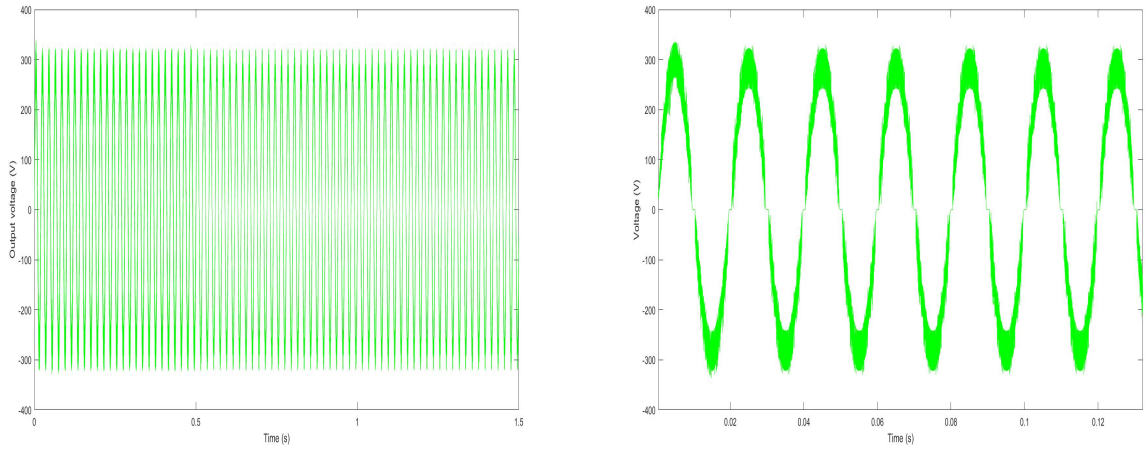

Figure 3.37: Output voltage at PCC- case of added loads

Output current

The output current at PCC during this scenario was also measured. The results are illustrated below.

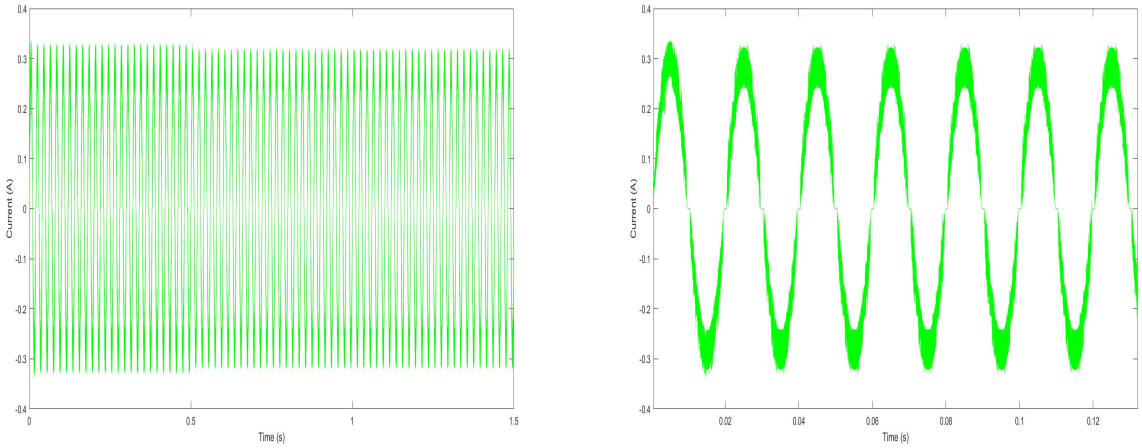

Figure 3.38: Output current at PCC- case of added loads

As in every scenario, the output of each VSI was also measured before filtering. The voltage waveforms are shown below.

Output voltage of VSIs

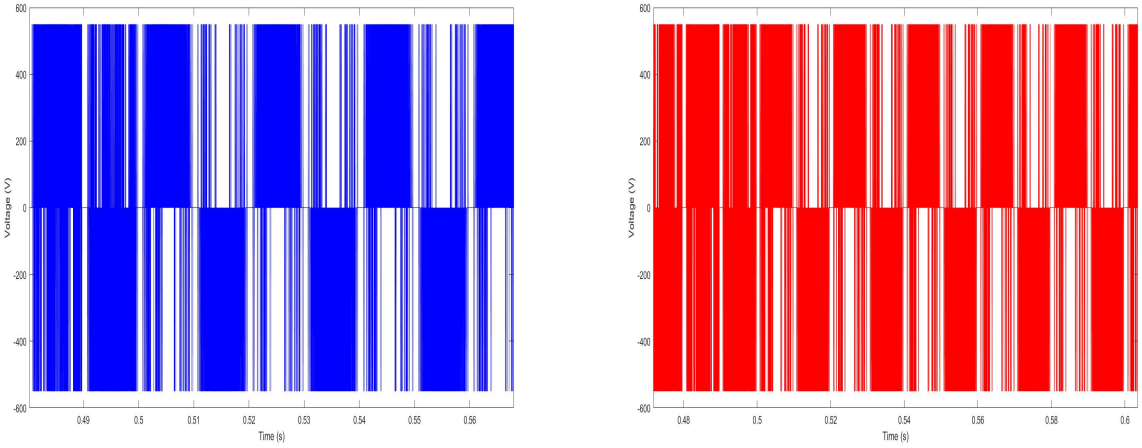

(a) Inverter voltage - VSI 1

(b) Inverter voltage - VSI 2

Figure 3.39: Inverter voltage - Case of added loads

The sine waves of inverter voltages after filtering are illustrated in the figures below.

Filtered output voltage VSI 1

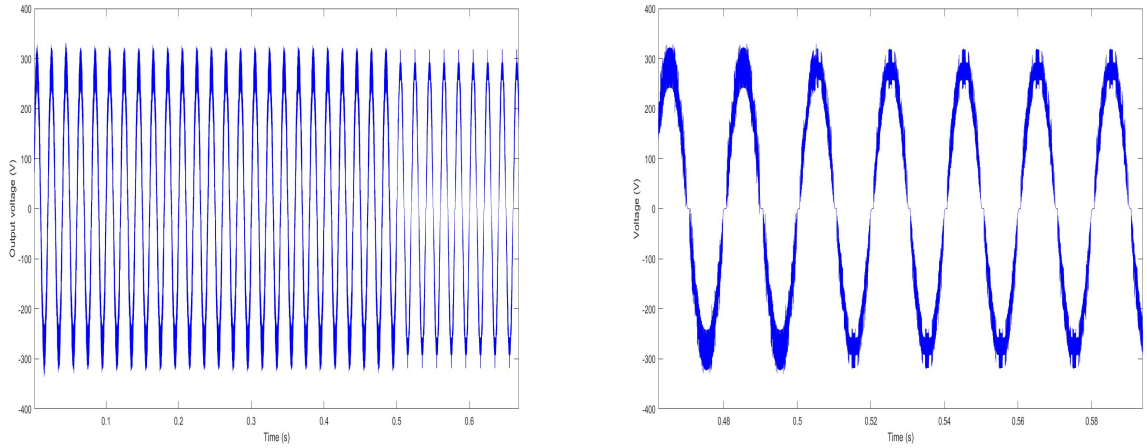

Figure 3.40: Filtered inverter output voltage - VSI 1

Filtered output voltage - VSI2

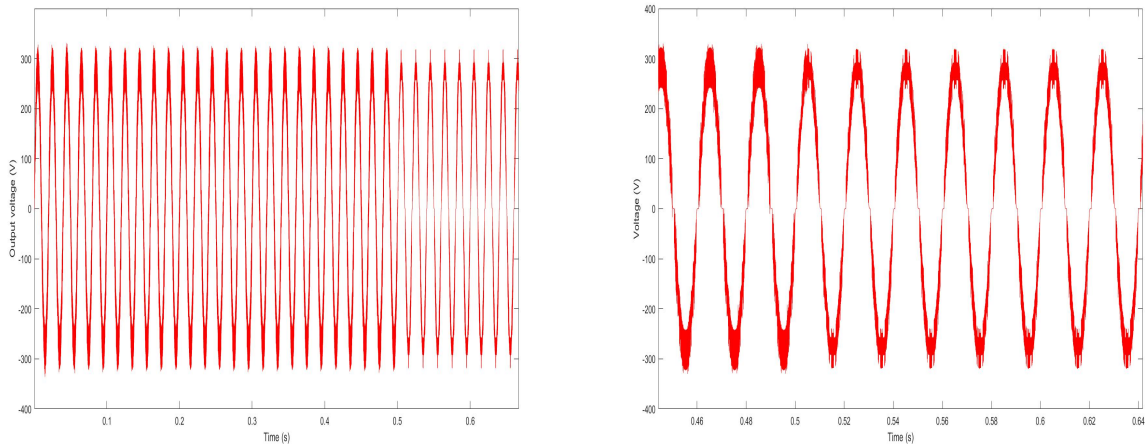

Figure 3.41: Filtered inverter output voltage - VSI 2

Current of VSIs

In order to see the effect of load addition on the behavior of DGs, and hence the MG. Output current of both VSIs was measured for the duration of the testing. The results are illustrated below.

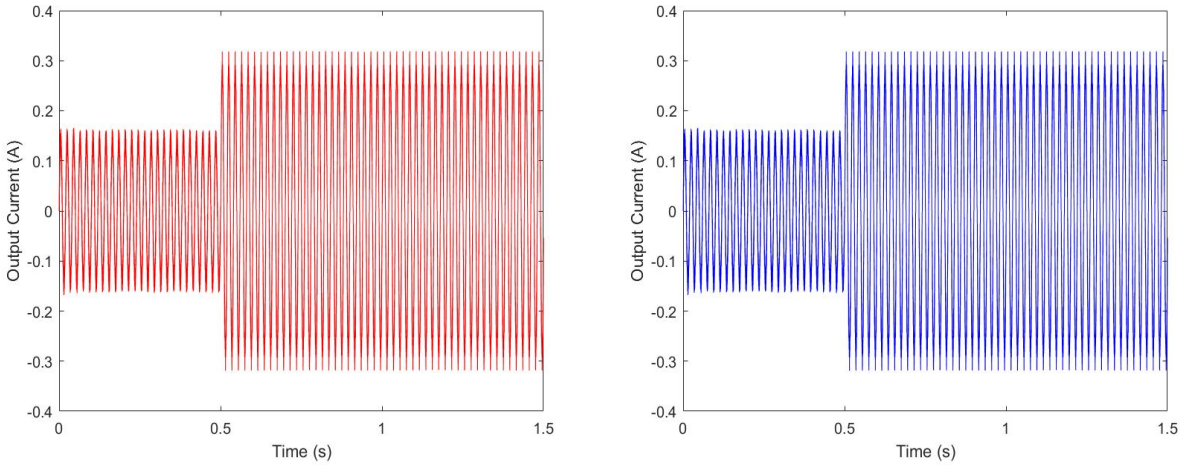

Figure 3.42: Inverters output current

Total harmonic distortion

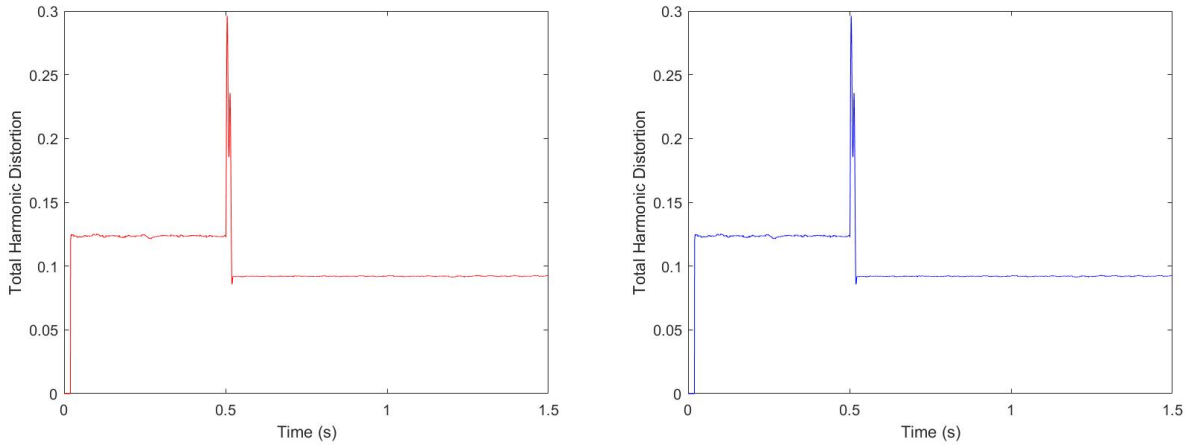

(a) THD of DG1 (b) THD of DG2

Figure 3.43: Total Harmonic Distortion of the MG

Active power

The effect of load addition to the MG can also be seen in the active power delivered by the VSIs. The corresponding results are illustrated below.

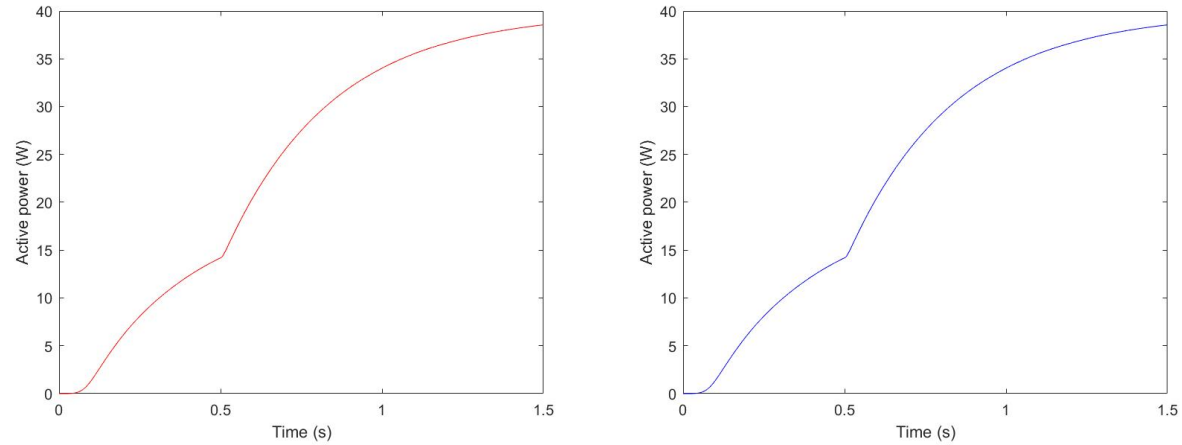

(a) Active power of DG1 (b) Active power DG2

Figure 3.44: Active power of the MG

Reactive power

The DGs reactive power results are illustrated below.

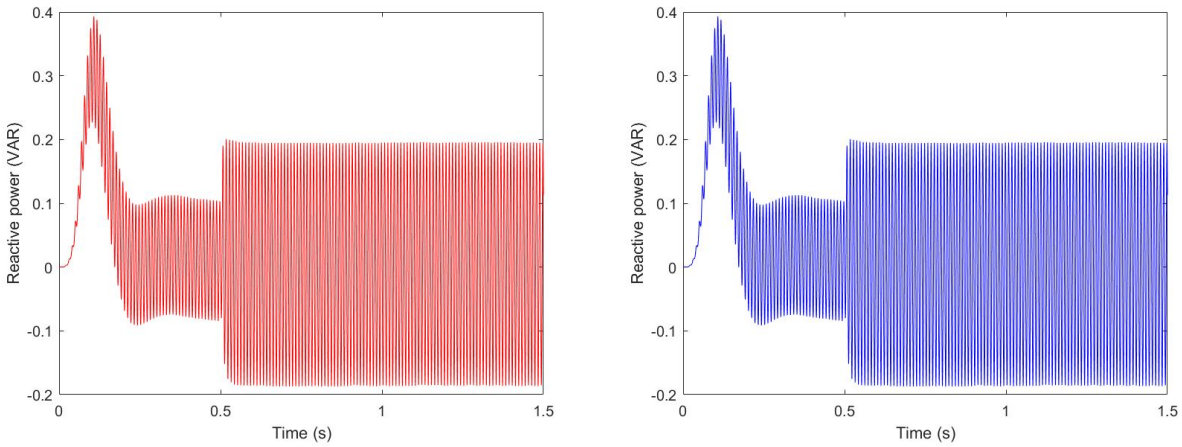

(a) Reactive power of DG1 (b) Reactive power of DG 2

Figure 3.45: Reactive power of the MG

Frequency

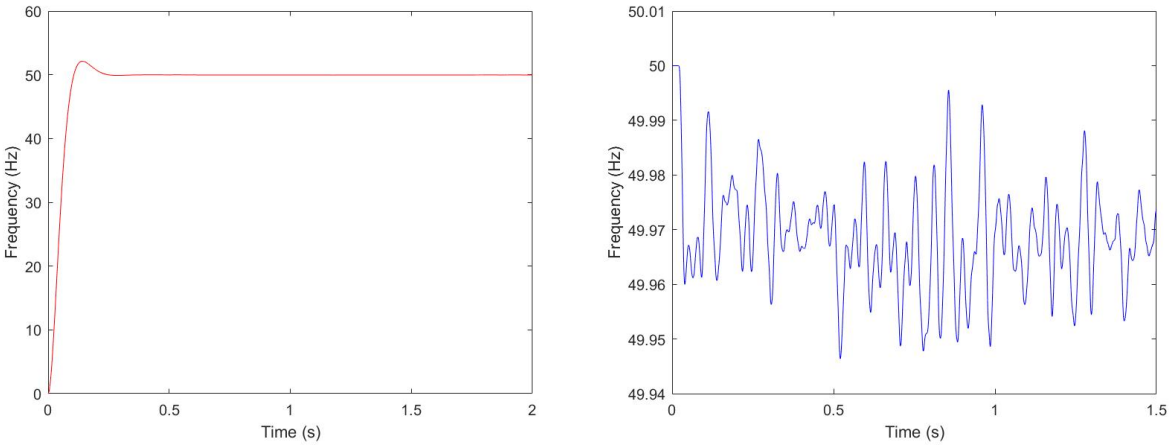

(a) Using SOGI-PLL (b) Using PLL

Figure 3.46: Frequency of the system

Discussion

A small voltage drop can be noticed in the voltage and current waveforms at the time the additional load is connected. Despite the disturbance, the voltage at the PCC and at each DG is always equal to the nominal value, $V_{peak} = 310$ V, and the frequency is kept around 50 Hz with minor fluctuations at the time of load addition.
The PLL measured frequency shows that the deviation doesn't exceed 0.1 % which falls under the permitted standard variation, which is 1%. The amplitude output current of the inverter is doubled after the second load is connected, which is reasonable as now the inverters will be feeding not one but two parallel loads of equal value. Furthermore, the power and reactive power are shared equally between both DGs and both notice an increasing in value after the second load is added. The reactive power fluctuates around 0 since both loads are resistive. The THD is around 0.13% and spikes for few miliseconds at the time the second load is connected to 0.3 % which is still considerably below the allowed maximum values of 5%. After simulating the system, one can notice from the resulting graphs that under load disturbance as well, the MG controller achieved its purpose.

3.2.5 Disconnected DGs

Testing under different load conditions is not enough to determine the system's robustness to change. In order to safely say that the controller is efficient under all circumstances, the system must be tested under disturbances in the generation as well. Which is why the MG was also tested under the case of disconnected DGs.
At time t = 0.5 s, DG 1 is connected to the network. The behavior of the system can be seen in the resulting graphs in the sections that follow.

Output voltage

The output voltage's measurement is shown in the waveforms that follow.

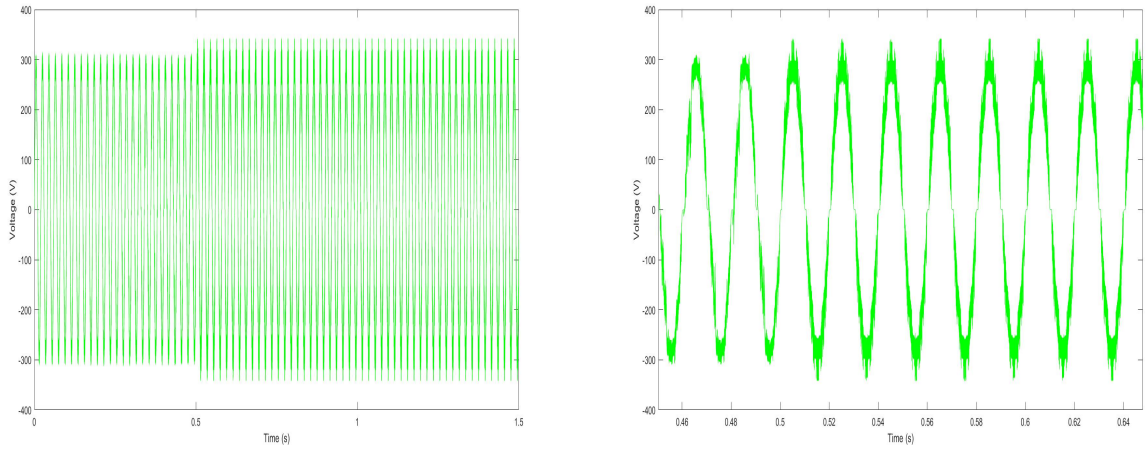

Figure 3.47: Output voltage at PCC - Disconnected DGs

Output current

The output current at PCC can be seen in the waveform below.

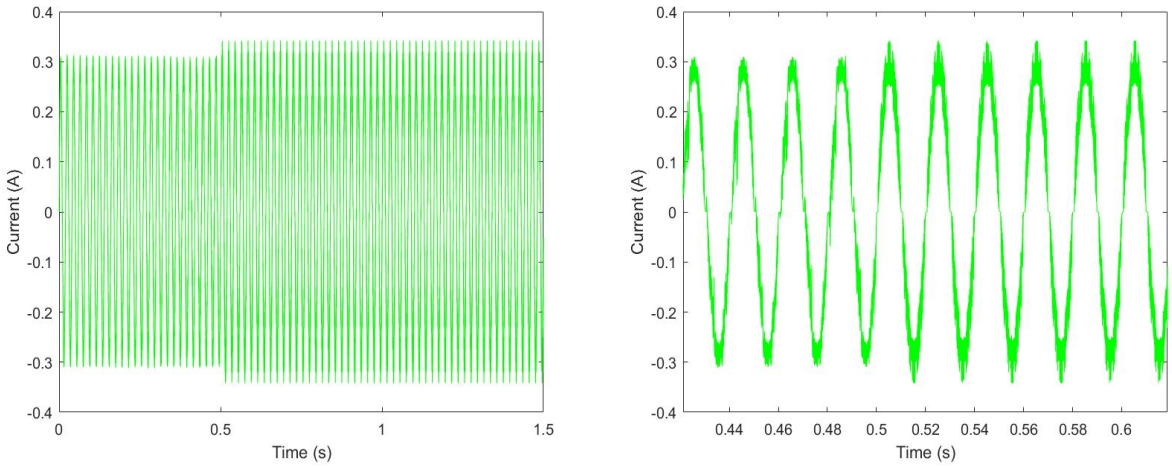

Figure 3.48: Output current at PCC - Disconnected DGs

Similar to the previous carried out tests, the pre-filtered voltage output of each inverter was measured.

Output voltage of VSIs

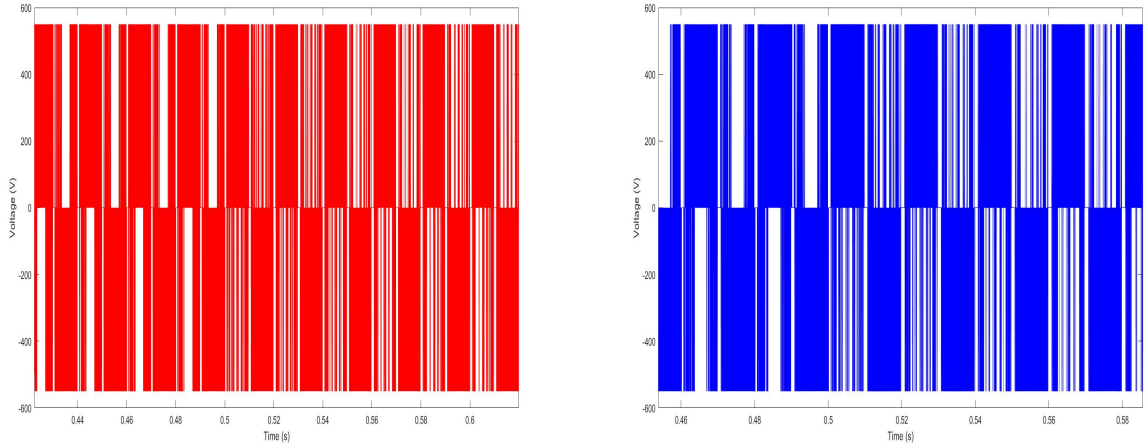

(a) Inverter voltage - VSI 1

(b) Inverter voltage - VSI 2

Figure 3.49: Inverter voltage- Case of disconnected DGs

After the LC filtering, a sine voltage is obtained. The resulting inverter voltages can are illustrated in the following figures.

Filtered inverter output voltage - VSI 1

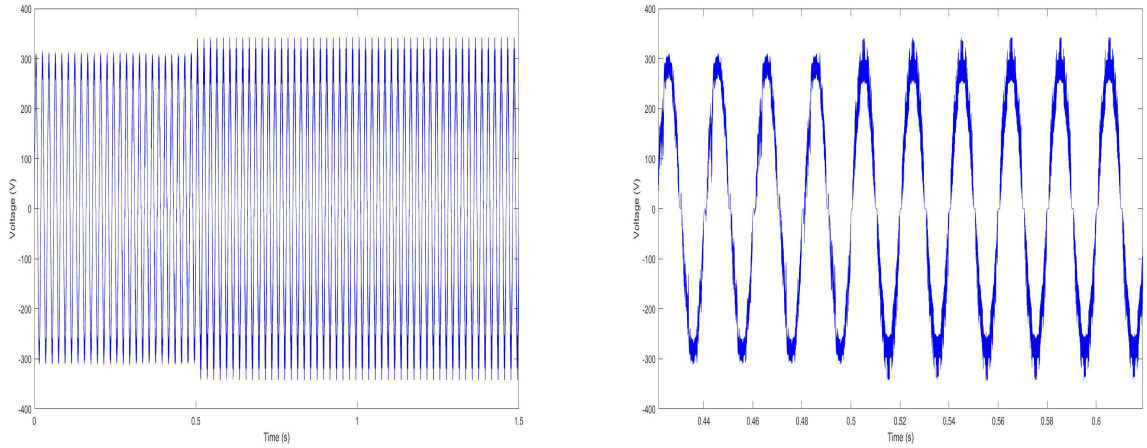

Figure 3.50: Filtered inverter output voltage VSI 1

Filtered inverter output voltage - VSI 2

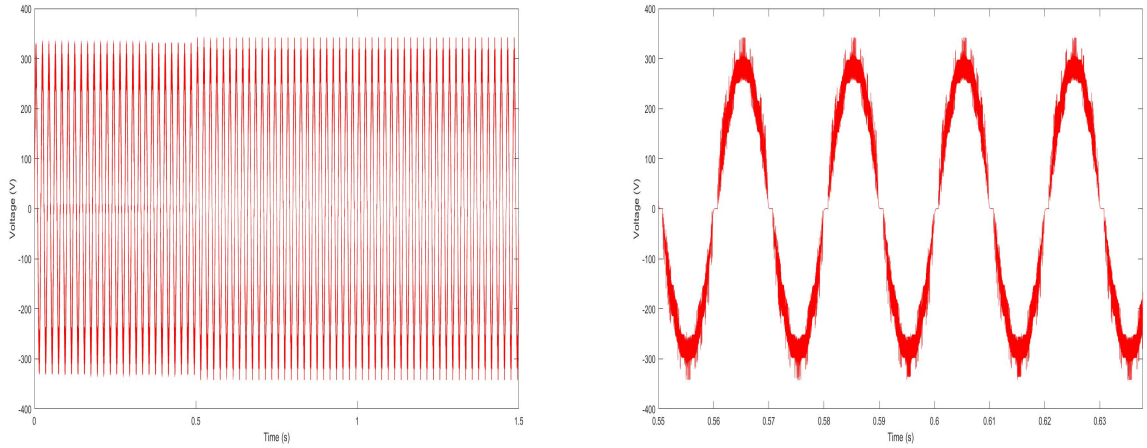

Figure 3.51: Filtered inverter output voltage VSI 2

The resulting inverter output current graphs are shown in the waveforms that follow.

Current of the VSIs

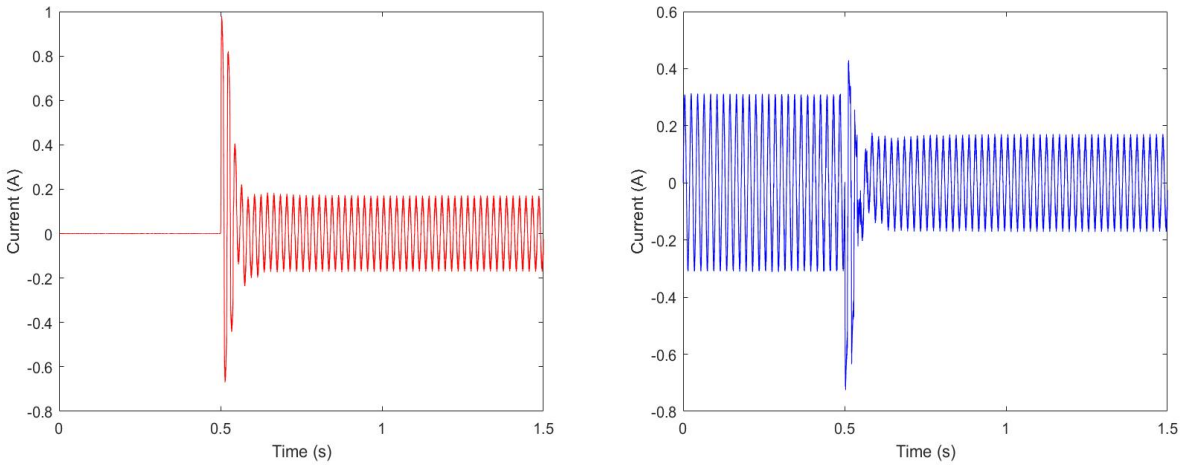

(a) Current of DG1 (b) Current of DG2

Figure 3.52: Inverter output current - case of disconnected DG

Total Harmonic Distortion

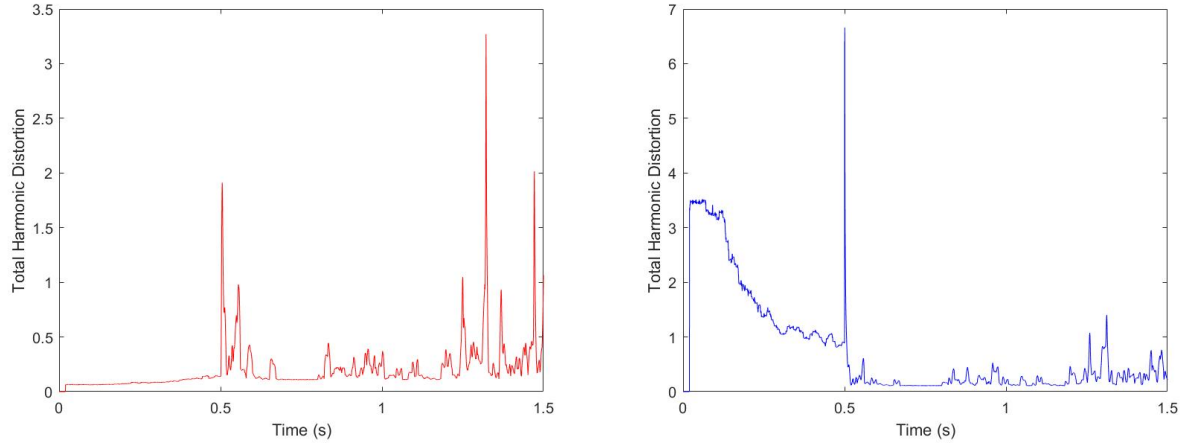

(a) THD of DG1 (b) THD of DG2

Figure 3.53: THD of the system - case of disconnected DGs

Active power

To further see the effect of adding DGs to the system, active power in both DGs was measured. Results are shown below.

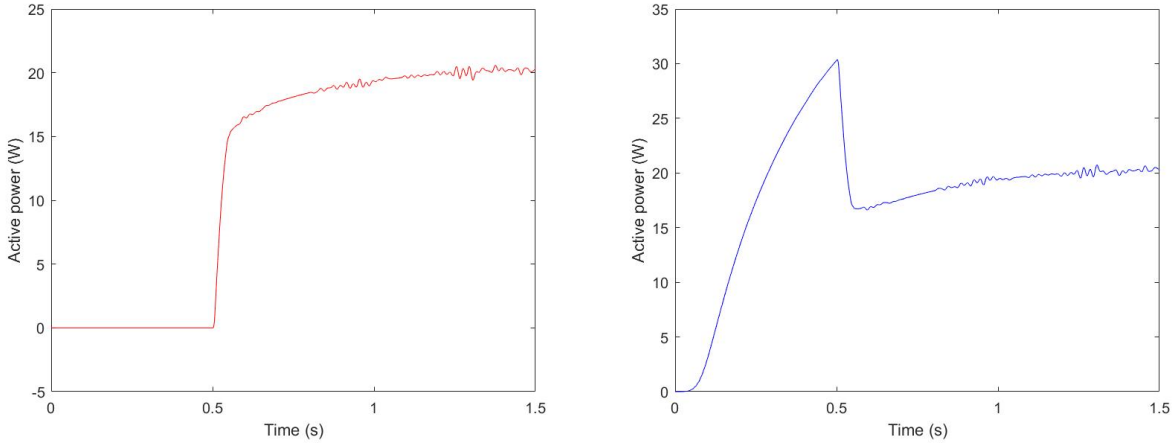

(a) Active power of DG1 (b) Active power of DG2

Figure 3.54: Active power of the MG

Reactive power

To further see the reaction of the system to adding DGs, reactive power in both DGs was measured. Results are shown below.

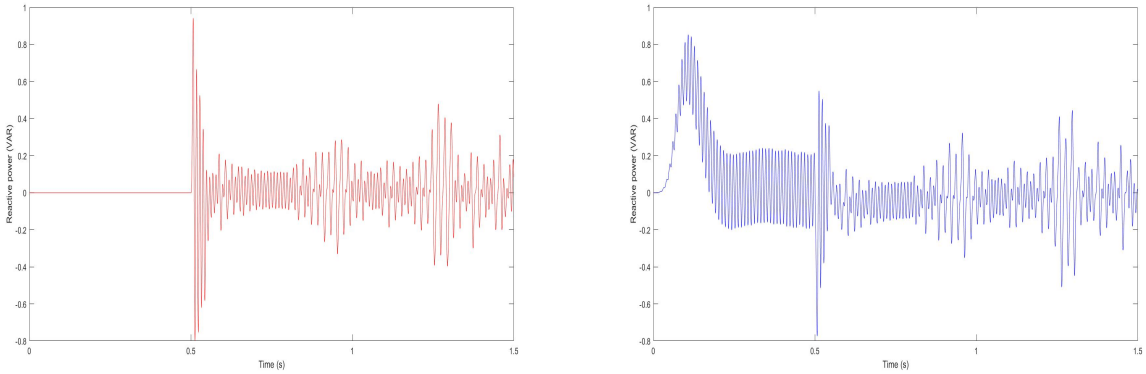

(a) Reactive power of DG1 (b) Reactive power of DG2

Figure 3.55: Reactive power of the MG

Frequency

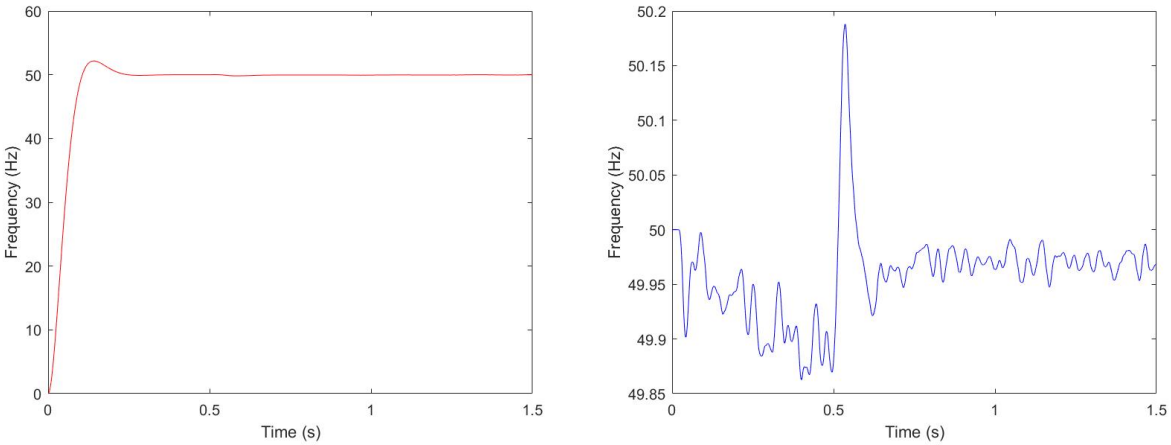

(a) Using SOGI-PLL (b) Using PLL

Figure 3.56: Frequency of the MG

Discussion

A minor increasing in amplitude can be noticed in the voltage and current waveforms at the moment the second DG (DG1) is connected to the network. Regardless of the disturbance, the voltage at the PCC and at each DG is equal to the nominal value, V_{peak} = 310 V, and the frequency is kept around 50 Hz with minor fluctuations.
The PLL measured frequency shows that the deviation doesn't exceed 0.1 % which falls under the permitted standard variation, which is 1%. The interesting change that occurs at the time the other DG is connected can be noticed in the VSIs output current. In DG1, the output current is 0 until the instant t= 0.5 s which is when the connection to the system occurs. On the other hand, the current in DG2 is twice as much the current it produces after the DG1 is added to the MG. This only demonstrates that there is a proper current-sharing between DGs, as they share the load equally. Furthermore, the power and reactive power also have a similar change. Both active and reactive power of DG1 are equal to zero before it is connected to the system. And similar to current, the second DG produces twice as much active power before it is aided with DG1.
This means that proper power-sharing is also ensured. The reactive power fluctuates around 0 since the load is not inductive. The THD is around 3.5% in DG2 before the second DG is added. At the moment of connection, THDs spike in both DGs, after which it drops to around 0.3 in both, which is considerably below the allowed maximum values of 5%. After simulating the system under the condition of generation disturbance, one can notice from the resulting graphs that under this scenario as well, the MG controller achieved its purpose.

3.2.6 Grid connection

The last case the system was tested under was the grid-connection. Despite the fact that the proposed system was designed to be robust during islanded mode only, a grid-connection simulation was added to showcase the necessity of the remaining control levels to achieve a good power management in the case of grid-tied operation.

Output voltage

The measurement of the output voltage at the PCC gave the following results:

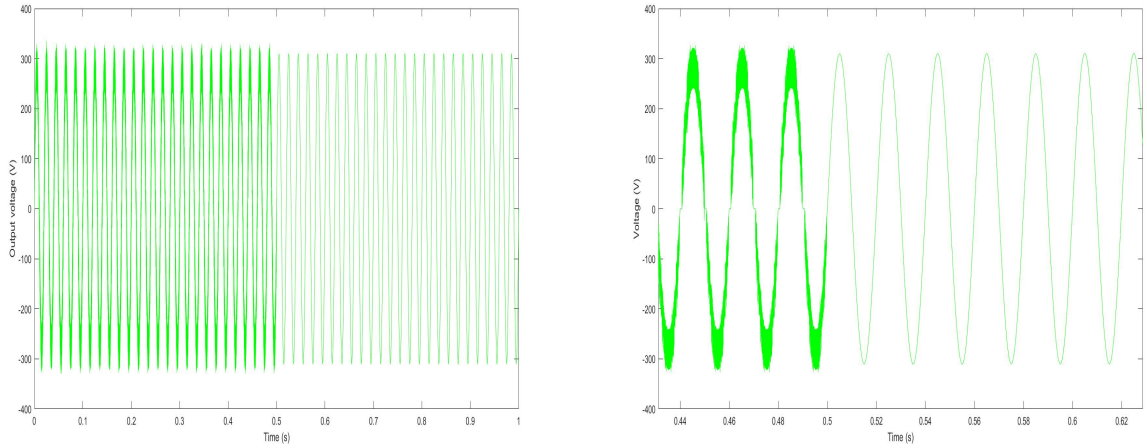

Figure 3.57: Output voltage at PCC - Case of grid-connection

Output current

The current flowing through the load is shown in the waveforms that follow:

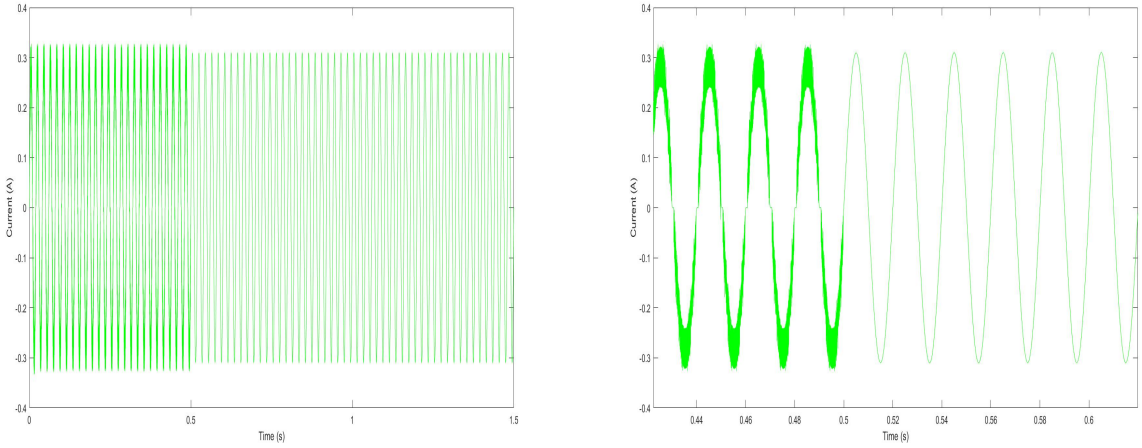

Figure 3.58: Output current at PCC - Case of grid-connection

The unfiltered output voltage of each DG's inverter can be seen in the following figures:

Output voltage of VSIs

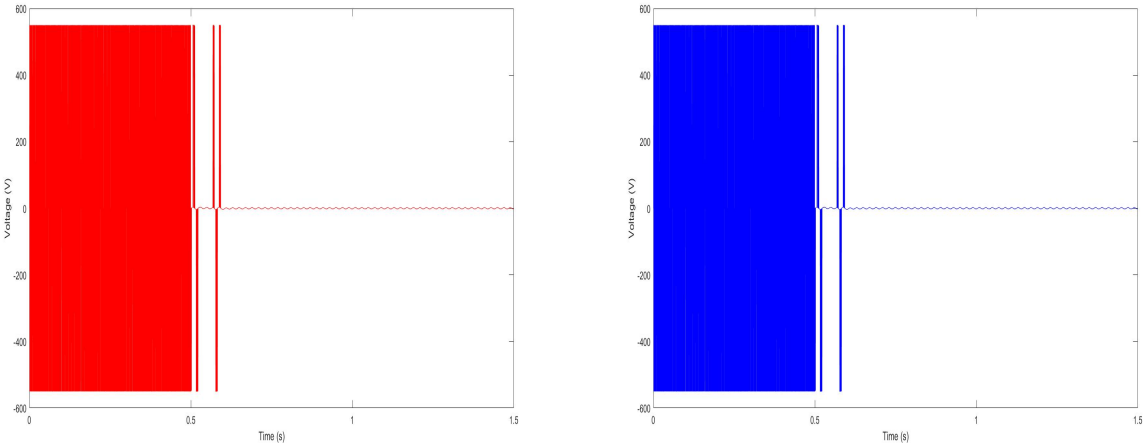

(a) Inverter voltage - VSI 1

(b) Inverter voltage - VSI 2

Figure 3.59: Inverter voltage - Case of grid-connection

The resulting inverter voltage after filtering for both VSIs is shown in the waveforms below.

Filtered voltage output of VSI 1

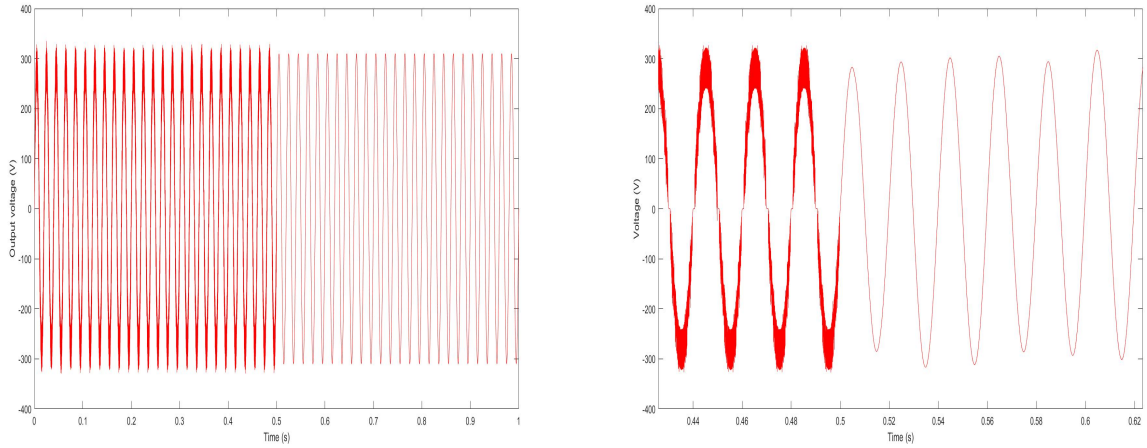

Figure 3.60: Filtered output voltage of VSI 1

Filtered voltage output of VSI 2

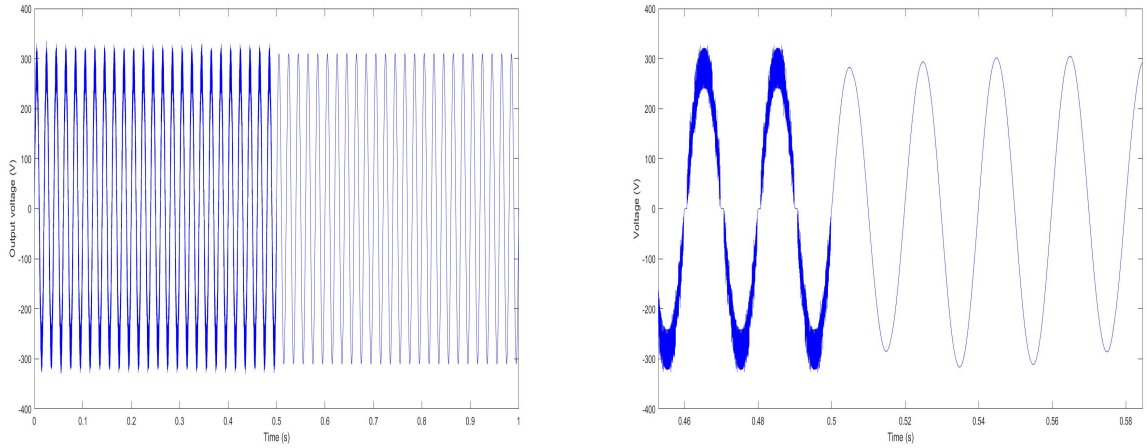

Figure 3.61: Filtered output voltage of VSI 2

The output current of the filtered inverter signals can be seen in the figures that follow.

Current of the VSI

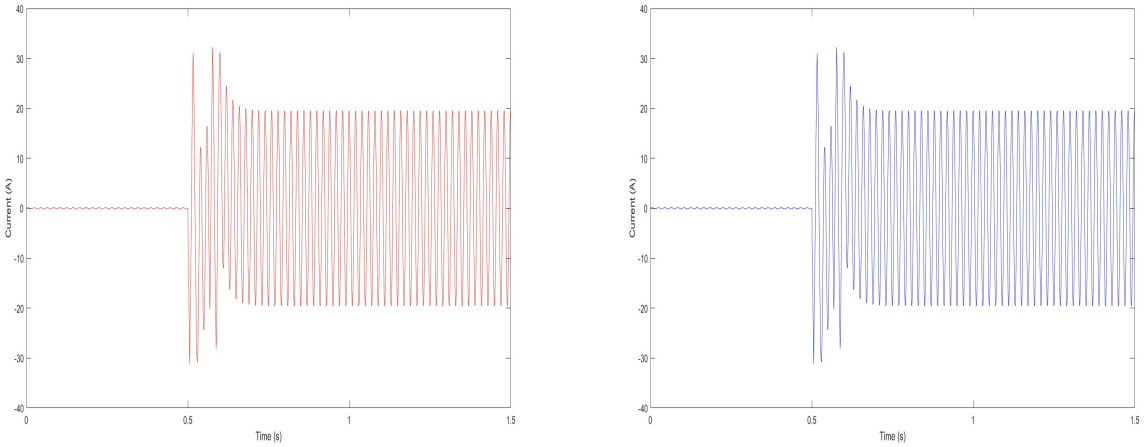

(a) Output current of DG1 (b) Output current of DG2

Figure 3.62: Output current of VSIs

Total Harmonic Distortion

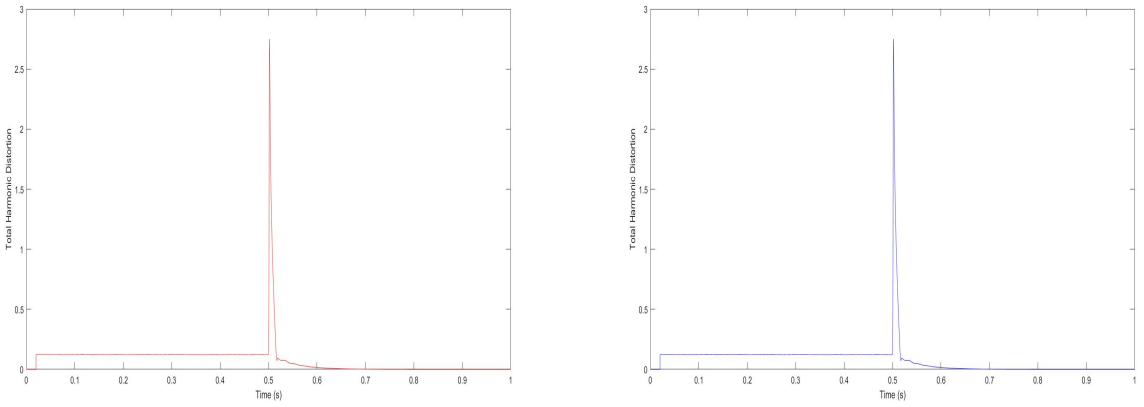

(a) THD of DG1 (b) THD of DG2

Figure 3.63: THD of the MG

Active power

The effect of grid-connection on the power-flow can be seen in the active power waveforms of both DGs, as shown in the following figures.

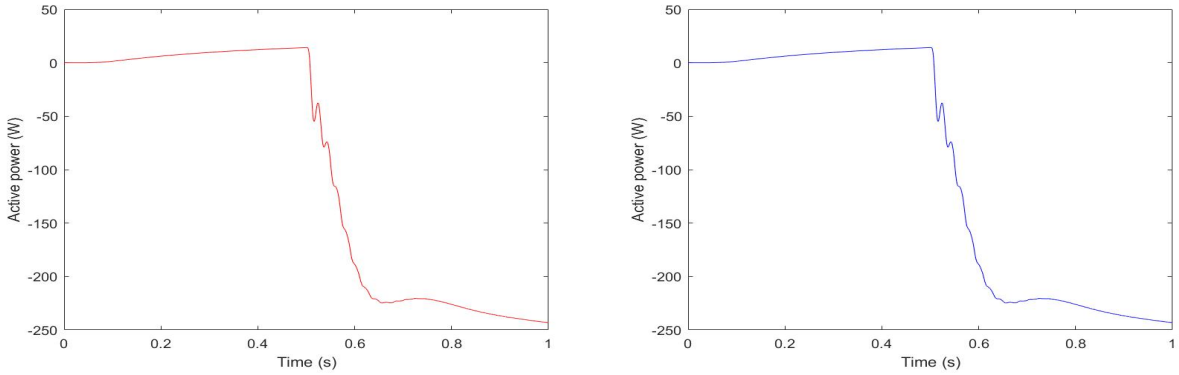

(a) Active power of DG1 (b) Active power of DG2

Figure 3.64: Active power of the MG

Reactive power

The effect of grid-connection on the power-flow can be seen in the reactive power waveforms of both DGs, as illustrated below.

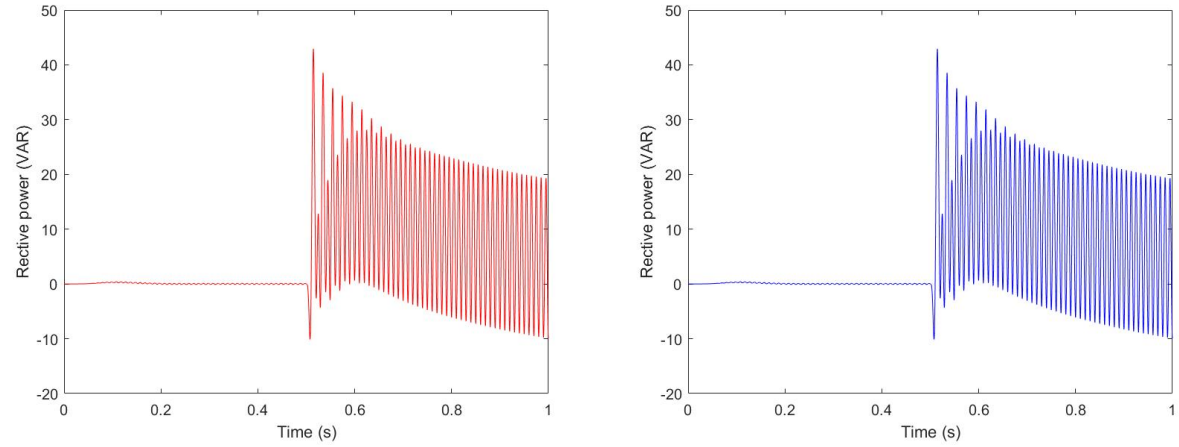

(a) Reactive power of DG1 (b) Reactive power of DG2

Figure 3.65: Reactive power of the MG

Frequency

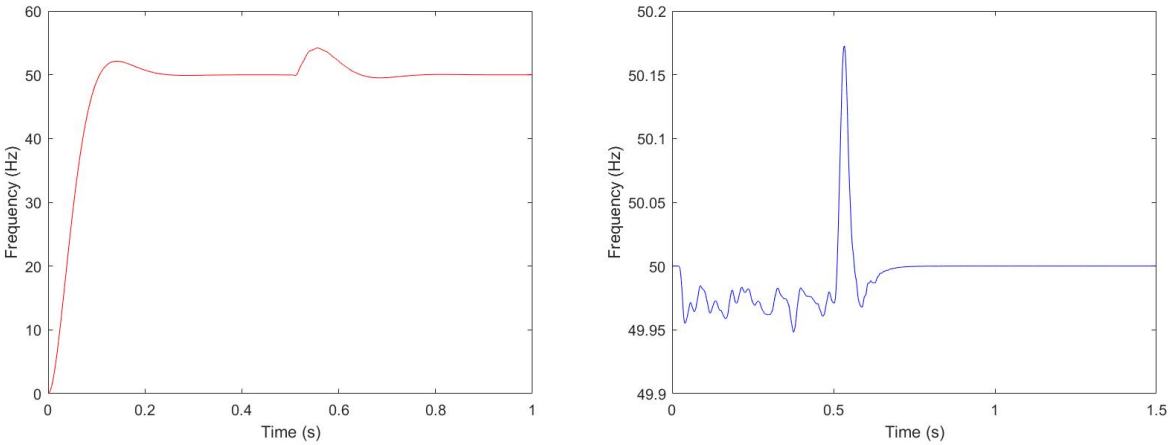

(a) Using SOGI-PLL (b) Using PLL

Figure 3.66: Frequency of the MG

Discussion

After the grid connection is established, the output voltage and current at the PCC become purely sinusoidal. The voltage amplitude at the PCC and at each DG remains equal to the nominal value, $V_{peak} = 310$ V, and the frequency is kept around 50 Hz with spikes at the time the grid connection is established.
The PLL measured frequency shows that the deviation doesn't exceed 0.4 % which falls under the permitted standard variation, which is 1%. Similarly to the PCC, the filtered voltage of both VSIs becomes purely sinusoidal at the time the MG becomes connected to the grid. While the unfiltered output voltage is reduced to a very small value at 0.5 s, which is, again, the time the MG is connected to the utility grid. Furthermore, the current output of each VSI increases substantially after the connection, before which it was fluctuating around 0.3 A. In addition to that, active power of each DG becomes negative after the connection, as though the VSIs act as loads to the grid. The THD is around 0.02% which is considerably below the allowed maximum values of 5% and only spikes at the moment the grid connection is established.
These results only further confirm the need to a secondary and tertiary control levels to ensure a proper energy management system in the grid-tied operation mode of the MG.

Conclusion and future works

Due to the increasing load demand and the strict regulations on carbon footprint, RES have become the new trend in energy generation, thanks to their 0 carbon emission and their reliance on natural resources. However, one major issue RES systems suffer from is their intermittent generation and need for power electronics converters before they can be connected to the main utility grid.
To solve this problem, MGs are introduced.

However, MGs have their own issues to deal with. As they are comprised of RES, they also suffer from unreliability as they rely on sources that are subject to changes depending on the environment. To this end, a hierarchical control strategy is used to ensure stable and reliable power in MGs, both in their islanded and grid-connected mode.

In the islanding mode of operation of MGs, the demand power should be shared among the different DGs considering their capacity to ensure balance and longer life-time of the DGs in use.

In this work, the implementation of the primary control based on the droop control method in islanded MG has been presented. The proposed control scheme was used to adjust the voltage frequency and amplitude of the VSIs, in order to provide the load-demand active and reactive power.

In chapter 1, a complete overview of MGs was presented, including definition, different MG configurations, advantages, and architectures, in addition to industry application. The hierarchical control of AC MG, including primary, secondary, and tertiary control levels were described along the different control strategies used in each level.

In chapter 2, the proposed power-sharing scheme design is described in details. The architecture of the proposed primary level is presented, along with the equations of each block and the values of the parameters used in the system. SOGI-PLL filter is introduced, with a comprehensive overview and a schematic diagram of the filter design.

In chapter 3, the Simulink model of the system is presented. Followed by the numerical

simulation results illustrating the system's response under different scenarios. The simulation results of the proposed MG power-sharing control demonstrated that the controller design achieved its primary purposed, which is proper active and reactive power in the DGs regardless of the load conditions. Furthermore, the voltage and frequency of the system are kept stable and equal to the nominal values, even in the case of disturbances. The system's response to grid-connection showed the necessity to a secondary and tertiary control levels to ensure stable and proper energy management in the case of grid-tied operation mode.

For future work, the current MG system can be expanded to operate in the grid-tied mode as well, by adding the secondary and tertiary control levels. Furthermore, to have a more accurate MG behavior, the DC DGs can be replaced by real DGs, such as PVs and wind turbines, in addition to Energy storage systems, ESS, to ensure the system's autonomy, since the RES used are intermittent in nature.

Bibliography

[1] Nicolae Scarlat et al. "Renewable energy policy framework and bioenergy contribution in the European Union – An overview from National Renewable Energy Action Plans and Progress Reports". In: *Renewable and Sustainable Energy Reviews* 51 (2015), pp. 969–985. ISSN: 1364-0321. DOI: https://doi.org/10.1016/j.rser.2015.06.062. URL: https://www.sciencedirect.com/science/article/pii/S1364032115006346.

[2] Bartosz Fortuński. "Sustainable Development and Energy Policy: Actual CO2 Emissions in the European Union in the Years 1997–2017, Considering Trade with China and the USA". In: *Sustainability* 12 (Apr. 2020), p. 3363. DOI: 10.3390/su12083363.

[3] J. Guerrero Hirsch Y. Parag. "Microgrids: A review of technologies, key drivers, and outstanding issue". In: *Renewable and Sustainable Energy Reviews. vol. 90, pp. 402-411* (2018).

[4] Joan Rocabert et al. "Control of Power Converters in AC Microgrids". In: *IEEE Transactions on Power Electronics* 27.11 (2012), pp. 4734–4749. DOI: 10.1109/TPEL.2012.2199334.

[5] Dan T. Ton and Merrill A. Smith. "The U.S. Department of Energy's Microgrid Initiative". In: *The Electricity Journal, vol. 25, no. 8, pp. 84-94,* (2012).

[6] Xuan Liu and Bin Su. "Microgrids — an integration of renewable energy technologies". In: (2008), pp. 1–7. DOI: 10.1109/CICED.2008.5211651.

[7] P. K. Rout B. Sahoo1 S.K. Routray. "AC, DC, and hybrid control strategies for smart microgrid application: A review". In: *International Transactions in Electrical Energy System.* (2020).

[8] Zhou Xue-song, Cui Li-qiang, and Ma You-jie. "Research on Control of Micro Grid". In: *2011 Third International Conference on Measuring Technology and Mechatronics Automation* 2 (2011), pp. 1129–1132.

[9] Hassan Nikkhajoei and Robert H. Lasseter. "Distributed Generation Interface to the CERTS Microgrid". In: *IEEE Transactions on Power Delivery* 24 (2009), pp. 1598–1608.

[10] Wei Yao et al. "An Improved Multiple-loop Controller for Parallel Operation of Single-phase Inverters with No Control Interconnections". In: *2007 IEEE Power Electronics Specialists Conference* (2007), pp. 448–452.

[11] Madureira AG Lopes JAP Moreira CL. "Defining control strategies for microgrids islanded operation". In: *IEEE Trans Power Syst* (2007. 916-924.).

[12] Hiroaki Kakigano, Yushi Miura, and Toshifumi Ise. "Low-Voltage Bipolar-Type DC Microgrid for Super High Quality Distribution". In: *IEEE Transactions on Power Electronics* 25 (2010), pp. 3066–3075.

[13] Vahidreza Nasirian et al. "Distributed Cooperative Control of DC Microgrids". In: *IEEE Transactions on Power Electronics* 30.4 (2015), pp. 2288–2303. DOI: 10.1109/TPEL.2014.2324579.

[14] Karel De Brabandere et al. "A Voltage and Frequency Droop Control Method for Parallel Inverters". In: *IEEE Transactions on Power Electronics* 22.4 (2007), pp. 1107–1115. DOI: 10.1109/TPEL.2007.900456.

[15] Z. Li Q. Zhou M. Shahidehpour and X. Xu. "Two-Layer Control Scheme for Maintaining the Frequency and the Optimal Economic Operation of Hybrid AC/DC Microgrids". In: *IEEE Transactions on Power Systems, vol. 34, no. 1, pp. 64-75,* (Jan 2019.).

[16] Tom Komarek et al. "Novel Ideas for Exploring Exploring Mars with CubeSats: Challenges and Possibilities". In: June 2013.

[17] Abderezak Lashab et al. "Space Microgrids: New Concepts on Electric Power Systems for Satellites". In: *IEEE Electrification Magazine* 8.4 (2020), pp. 8–19. DOI: 10.1109/MELE.2020.3026436.

[18] L. Berthoud E. Wertheimer and M. Johnson. "PocketRTG: a cubeSat scale radioisotope thermoelectric generator using COTS fuel". In: *Proc. 9th iCubeSat Workshop, 2015. [Online],* (Available: https://icubesat.org/papers/2015-2/2015-b-3-3/).

[19] Josep M. Guerrero et al. "Shipboard Microgrids: Maritime Islanded Power Systems Technologies". In: *PCIM Asia 2016; International Exhibition and Conference for Power Electronics, Intelligent Motion, Renewable Energy and Energy Management.* 2016, pp. 1–8.

[20] A. Vicenzutti; D. Bosich; G. Giadrossi.et al. "The role of voltage controls in modern allelectrical ships toward the all-electric ship". In: *IEEE Electrification Magazine.vol. 3, no. 2, pp. 49-65* (2015).

[21] "Microgrid project in Vienna". In: (Accessed May, 30th, 2022). URL: https://new.siemens.com/global/en/company/stories/infrastructure/2020/microgrid-project-in-vienna.html.

[22] *The long road around the world in 9 microgrids.* https://www.pv-magazine-india.com/2019/11/16/the-long-read-around-the-world-in-nine-microgrids/. Accessed May, 30th, 2022.

[23] *Hitachi ABB Power Grids enables greener mining with largest microgrid facility in Indonesia and Southeast Asia.* https://www.hitachienergy.com/news/press-releases/2021/02/hitachi-abb-power-grids-enables-greener-mining-with-largest-microgrid-facility-in-indonesia-and-southeast-asia. Accessed June, 9th, 2022.

[24] Mehrizi-Sani A Yazdanian M. "Distributed control techniques in microgrids". In: *IEEE Trans Smart Grid 2901-2909.* (2014).

[25] Malesani L Kazmierkowski MP. "Current control techniques for three-phase voltage-source PWM converters: a survey". In: *IEEE Trans Ind.Electron 691-703* (1998).

[26] J.M. Guerrero et al. "Output impedance design of parallel-connected UPS inverters with wireless load-sharing control". In: *IEEE Transactions on Industrial Electronics* 52.4 (2005), pp. 1126–1135. DOI: 10.1109/TIE.2005.851634.

[27] Ritwik Majumder et al. "Droop Control of Converter-Interfaced Microsources in Rural Distributed Generation". In: *IEEE Transactions on Power Delivery* 25.4 (2010), pp. 2768–2778. DOI: 10.1109/TPWRD.2010.2042974.

[28] Ritwik Majumder et al. "Angle droop versus frequency droop in a voltage source converter based autonomous microgrid". In: *2009 IEEE Power Energy Society General Meeting.* 2009, pp. 1–8. DOI: 10.1109/PES.2009.5275987.

[29] Madureira AG Lopes JAP Moreira CL. "Defining control strategies for microgrids islanded operation". In: *IEEE Trans Power Syst* (2007. 916-924.).

[30] Wenyuan Cao et al. "A Novel Power Sharing Scheme of Controlling Parallel-Operated Inverters in Islanded Microgrids". In: *IEEE Journal of Emerging and Selected Topics in Power Electronics* 9.5 (2021), pp. 5732–5746. DOI: 10.1109/JESTPE.2020.3048522.

[31] Josep M. Guerrero et al. "Hierarchical Control of Droop-Controlled AC and DC Microgrids—A General Approach Toward Standardization". In: *IEEE Transactions on Industrial Electronics* 58 (2011), pp. 158–172.

[32] Y. Khayat et al. "On the Secondary Control Architectures of AC Microgrids: An Overview". In: *IEEE Transactions on Power Electronics, vol. 35, no. 6, pp. 6482-6500* (June 2020).

[33] Meiqin Mao et al. "Multiagent-Based Hybrid Energy Management System for Microgrids". In: *IEEE Transactions on Sustainable Energy* 5.3 (2014), pp. 938–946. DOI: 10.1109/TSTE.2014.2313882.

[34] Fengji Luo et al. "Multiagent-Based Cooperative Control Framework for Microgrids' Energy Imbalance". In: *IEEE Transactions on Industrial Informatics* 13.3 (2017), pp. 1046–1056. DOI: 10.1109/TII.2016.2591918.

[35] Y. Hou L. Liang and D. J. Hill. "Design guidelines for MPC-based frequency regulation for islanded microgrids with storage, voltage, and ramping constraints". In: *IET Renew. Power Gener. vol. 11, no. 8, pp. 1200– 1210* (vol. 63, no. 9, pp. 5).

[36] Glielmo L Parisio A Rikos E. " A model predictive control approach to microgrid operation optimization". In: *IEEE Trans Control Syst Technol.;22(5):1813-1827* (IEEE Trans Control Syst Technol. 2014;22(5):1813-1827.).

[37] A. Bidram and A. Davoudi. "Hierarchical Structure of Microgrids Control System". In: *IEEE Transactions on Smart Grid, vol. 3, no. 4, pp. 1963-1976* (Dec. 2012).

[38] L.Meng et al. "Flexible System Integration and Advanced Hierarchical Control Architectures in the Microgrid Research Laboratory of Aalborg University". In: *IEEE Transactions on Industry Applications, vol. 52, no.2, pp. 1736-1749* (March-April 2016).

[39] Saeed Golestan et al. “Design and Tuning of a Modified Power-Based PLL for Single-Phase Grid-Connected Power Conditioning Systems”. In: *IEEE Transactions on Power Electronics* 27.8 (Aug. 2012), pp. 3639–3650. ISSN: 0885-8993.

[40] Bin Liu et al. “A Simple Approach to Reject DC Offset for Single-Phase Synchronous Reference Frame PLL in Grid-Tied Converters”. In: *IEEE Access* PP (June 2020), pp. 1–1. DOI: 10.1109/ACCESS.2020.3003009.

[41] Jorge Carreño et al. “HIL-Assessed Fast and Accurate Single-Phase Power Calculation Algorithm for Voltage Source Inverters Supplying to High Total Demand Distortion Nonlinear Loads”. In: *Electronics* 9 (Oct. 2020), p. 1643. DOI: 10.3390/electronics9101643.

[42] John Simpson-Porco, Florian Dörfler, and Francesco Bullo. “Synchronization and Power Sharing for Droop-Controlled Inverters in Islanded Microgrids”. In: *Automatica* 49 (June 2012). DOI: 10.1016/j.automatica.2013.05.018.